Synthesis, Characterization and Computational studies of copper(II) terpyridine-based metal-organic frameworks for the removal of emerging herbicide contaminant from aqueous solution

Adedibu C. Tella[a]; Sunday J. Olatunji[a,b]; Solomon O. Oloyede [b], Allen T. Gordon[c] Adeniyi S. Ogunlaja [c] ; Peter A. Ajibade*[b]

[a] *Department of Chemistry, P.M.B.1515, University of Ilorin, Ilorin, Kwara State, Nigeria*

[b] *Discipline of Chemistry, School of Agriculture and Science, University of KwaZulu-Natal, Private Bag X01, Scottsville 3209, South Africa*

[c] *Department of Chemistry, Nelson Mandela University, Gqeberha P.O. Box 77000, South Africa*

Supplementary Information

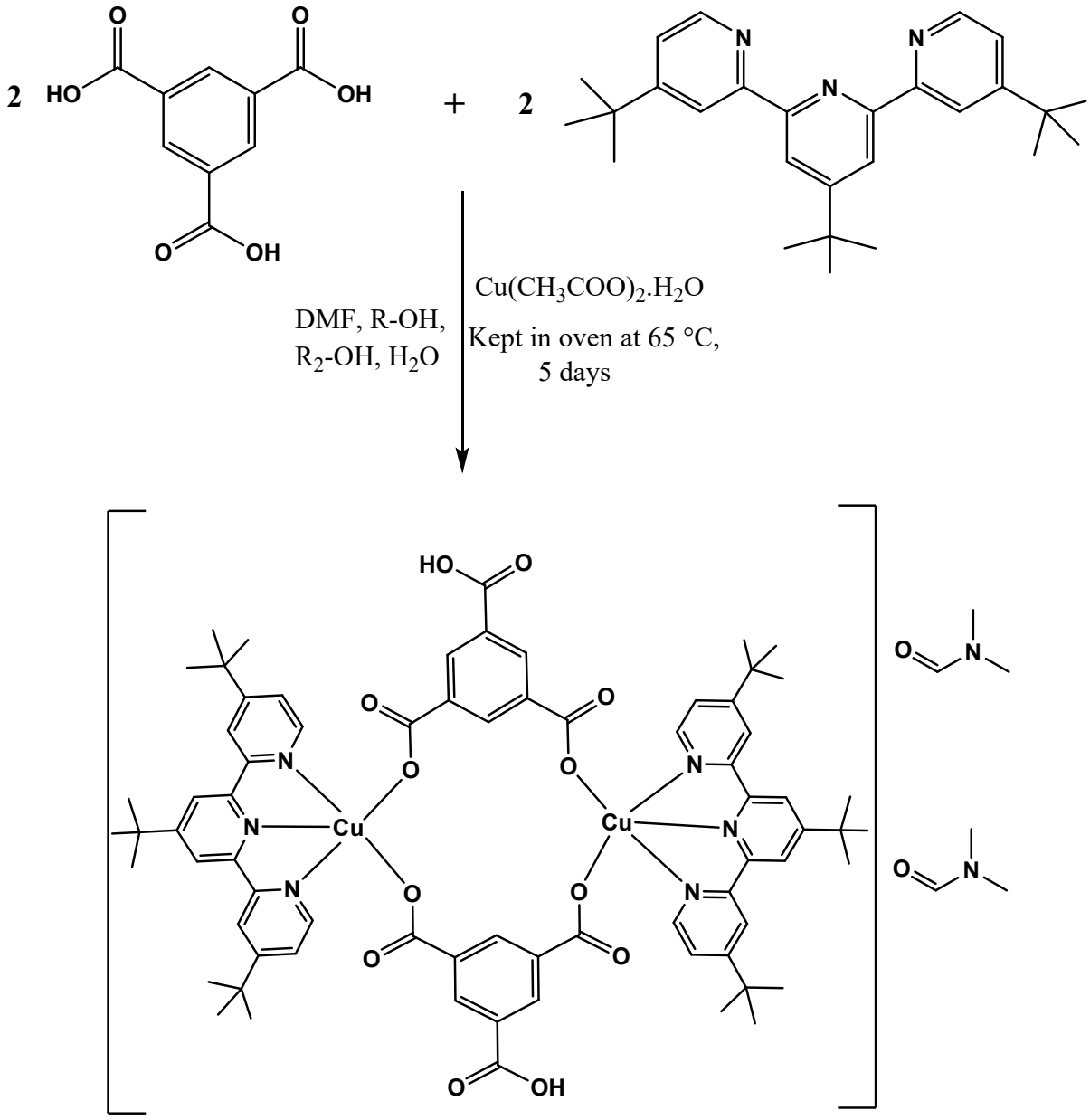

Scheme S1: Synthesis of $[Cu(btc)(N_3ttb)]_2 \cdot 2(DMF)$

Colour: Green, Yield: 82 %, M. pt.: >350 °C, Anal. Calcd M. wt.= 819.43 g/Smol. Anal. Found (Calcd) % for ($C_{42}H_{54}Cu_2N_5O_8$): C, 62.06 (61.48); H, 6.94 (6.63); N, 8.30 (8.54), FT-IR (ATR, cm^{-1}): 3447.8, 3097, 3063, 2952, 2866, 1654, 1606, 1558, 1472, 1431, 1386, 1345, 1248, 1177, 1092, 920, 887, 723, 682, 611 *m/z* (DMSO, %): 499.1711 (100.0%), 501.1711 (77.43 %), 424.2666 (47.79 %), 432.7401 (29.23 %), 500.1768 (28.24 %), 271.1092 (21.81%), 429.2433 (21.60 %), 502.1747 (20.95 %), 430.2446 (20.94 %), 433.7417 (18.00 %), 179.0165 (17.27 %), 503.1708 (15.83 %), 719.4337 (14.81 %), 425.2722 (14.32 %), 272.1093 (12.06 %), 523.2211 (10.05 %), 434.2423 (8.41 %), 747.4647 (7.75 %), 720.4379 (6.55 %), 495.2256 (6.18 %), 825.5411 (5.80 %), 525.2218 (5.09 %).

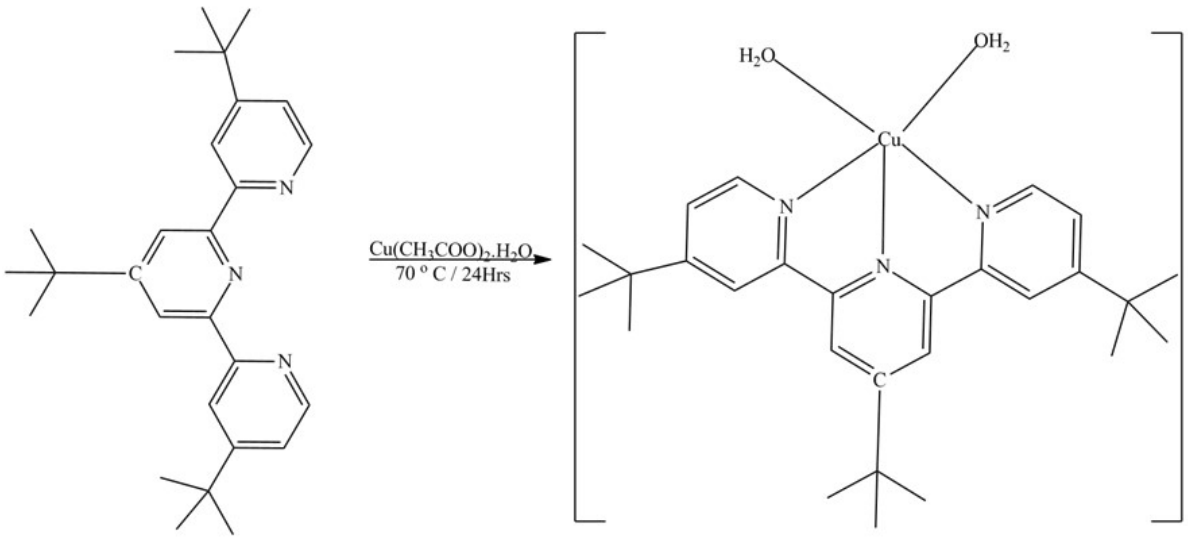

Scheme S2: Synthesis of [Cu(N_3ttb)(H_2O)]

Colour: Blue, Yield: 64 %, M. pt.: 292.5 °C, Anal. Calcd M. wt.= 501.16 g/mol. Anal. Found (Calcd) % for ($C_{27}H_{39}CuN_3O_2$): C, 64.78 (64.71); H, 7.34 (7.84); N, 8.45 (8.38), FT-IR (ATR, cm^{-1}): 2970, 1610, 1554, 1476, 1427, 1379, 1312, 1259, 1203, 1148, 1021, 916, 750, 670, *m/z* (DMF, %): 499.1864 (100.0%), 501.1852 (79.94%), 502.1887 (23.60%), 503.1845 (17.73%), 464.9663 (7.27%), 179.0205 (7.15%), 246.9361 (6.17%).

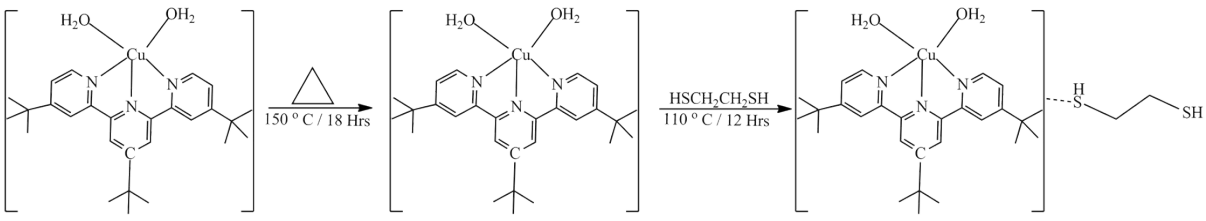

Scheme S3 Thiol-functionalization of [Cu(N_3ttb)(H_2O)$_2$]

Colour: Brown, Yield: 83 %, Anal. Found (%): C, 58.55; H, 8.18; N, 7.21; S, 15.25, IR (ATR cm^{-1}): 2952, 2899, 2866, 1699, 1625, 1584, 1517, 1476, 1408, 1244, 1110, 1077, 995, 924, 890, 842, 760, 730, 667

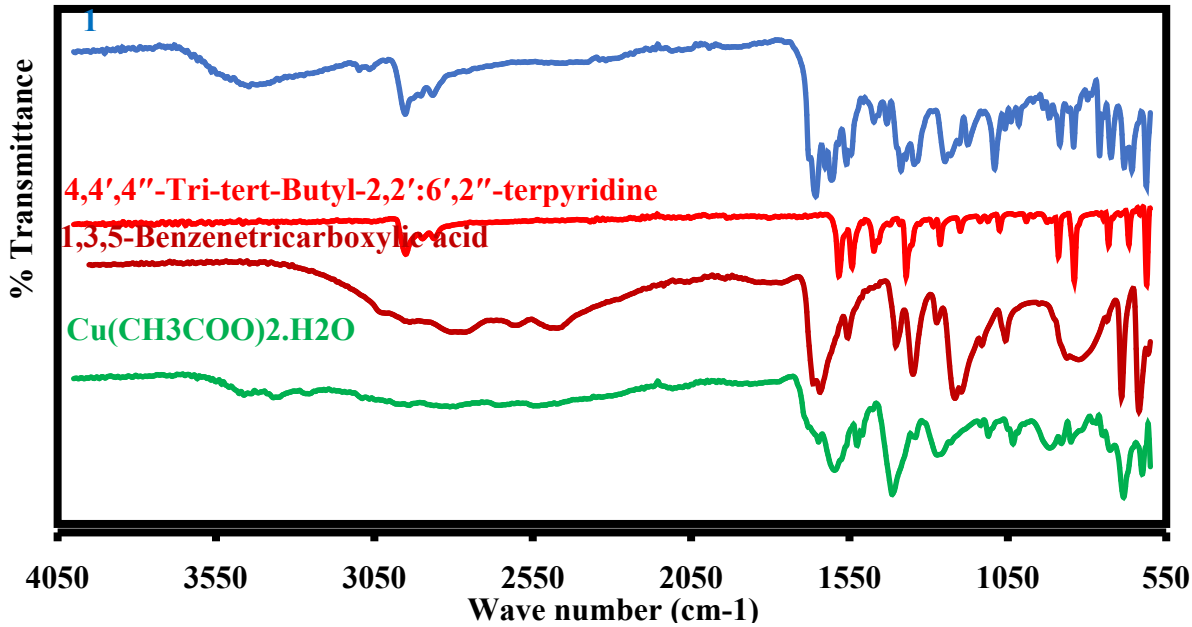

Figure S1: FT-IR spectra of 4,4′,4″-Tri-tert-Butyl-2,2′:6′,2″-terpyridine, 1,3,5-Benzenetricarboxylic acid, $Cu(CH_3COO)_2.H_2O$ and **1**.

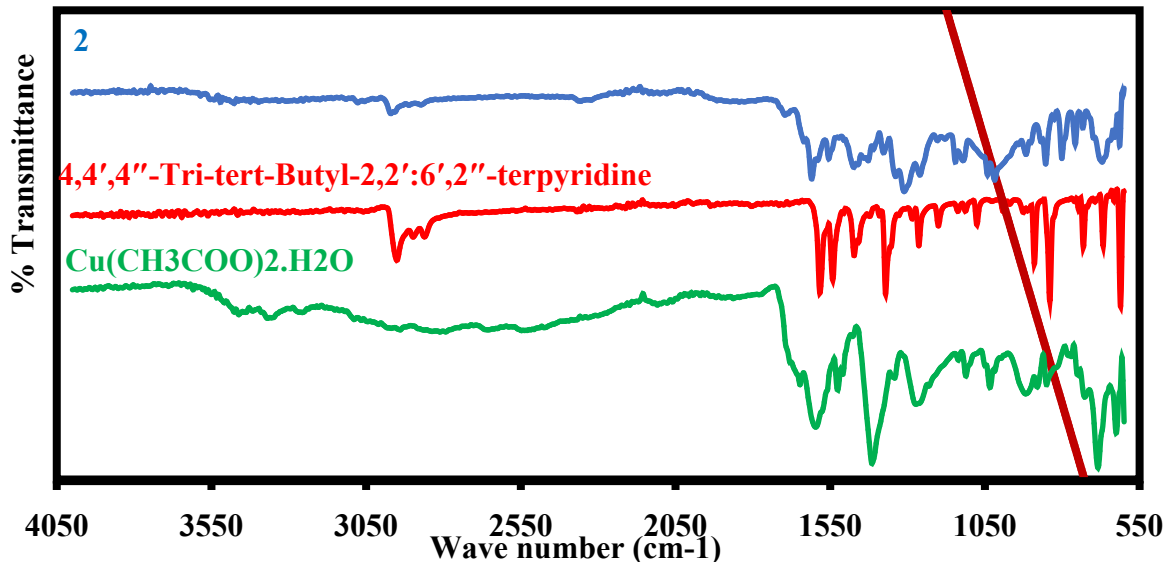

Figure S2: FT-IR spectra of 4,4′,4″-Tri-tert-Butyl-2,2′:6′,2″-terpyridine, $Cu(CH_3COO)_2.H_2O$ and **2**.

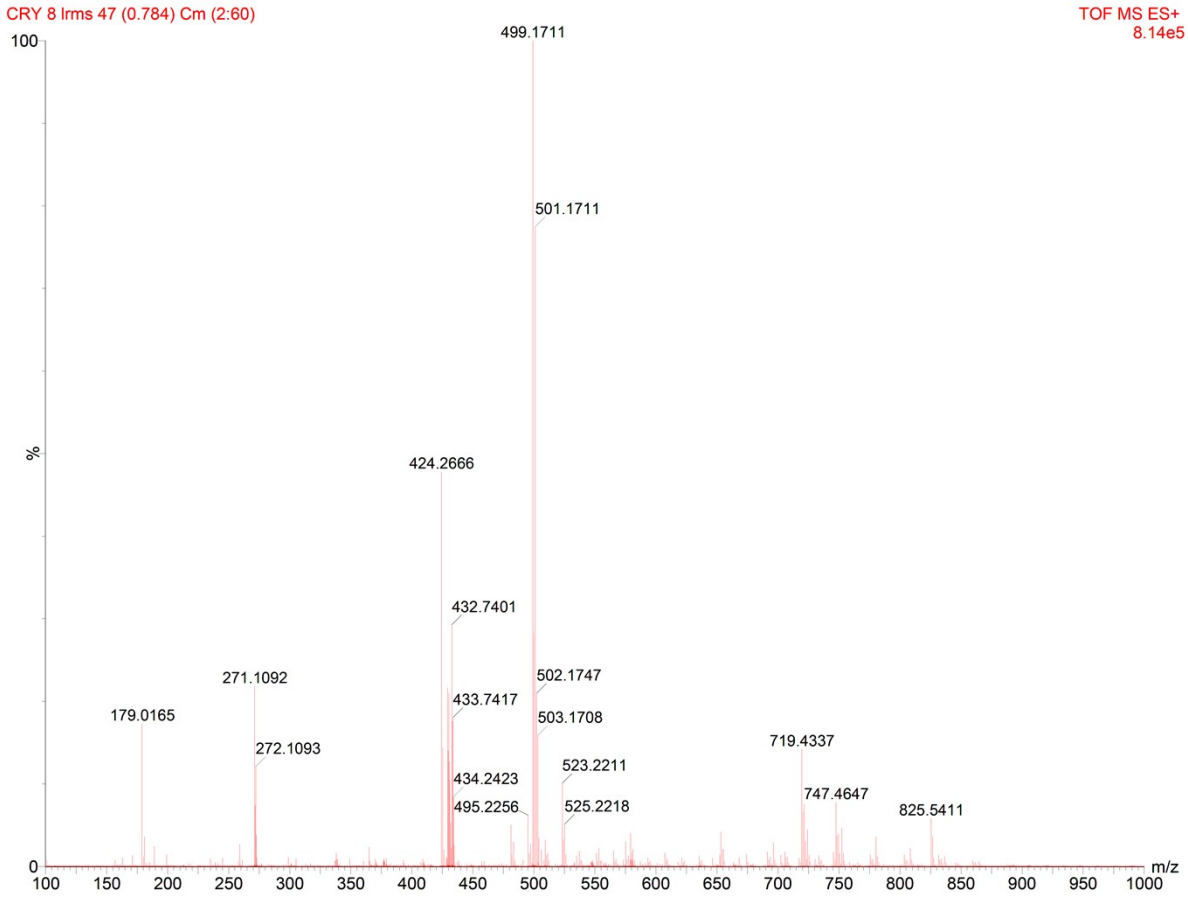

Figure S3: Mass spectra of **1**

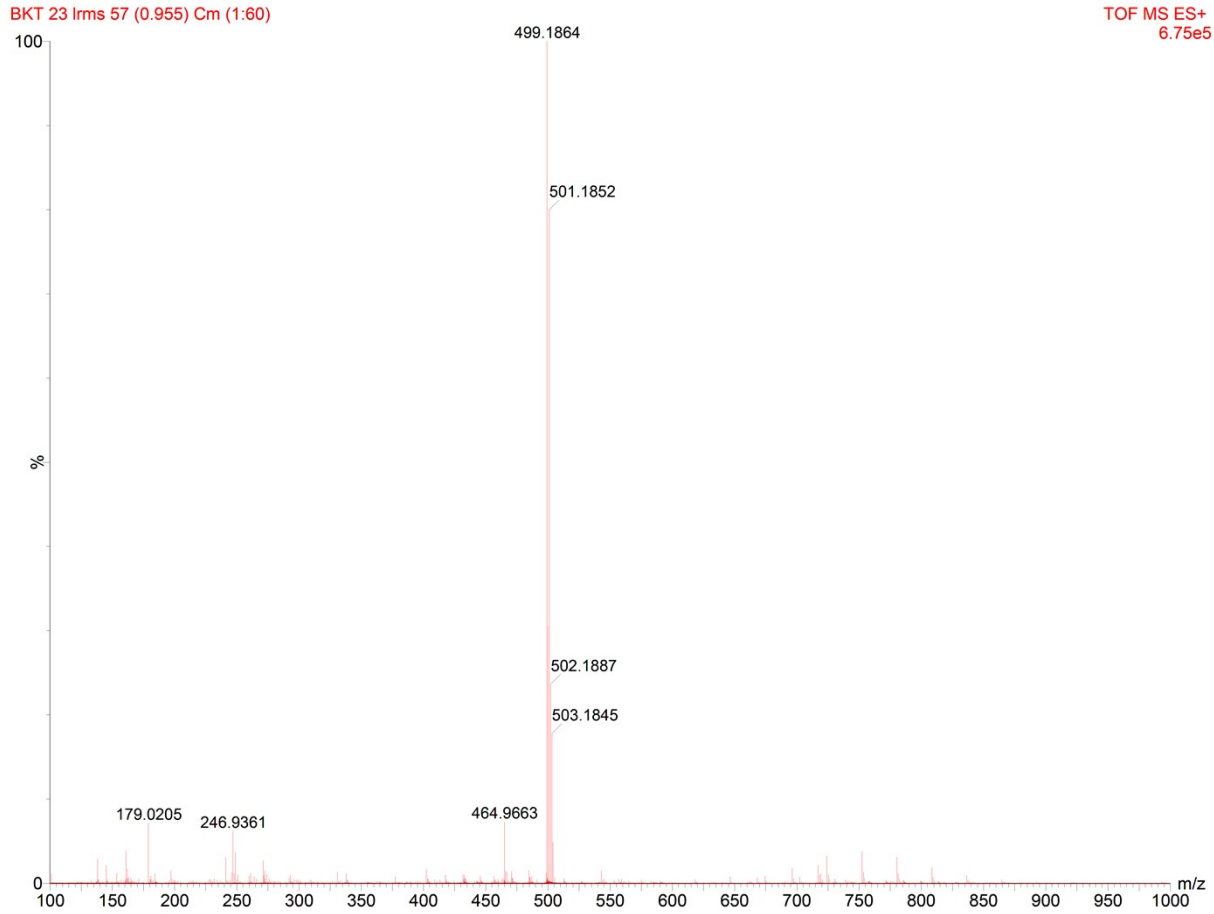

Figure S4: Mass spectra of **2**

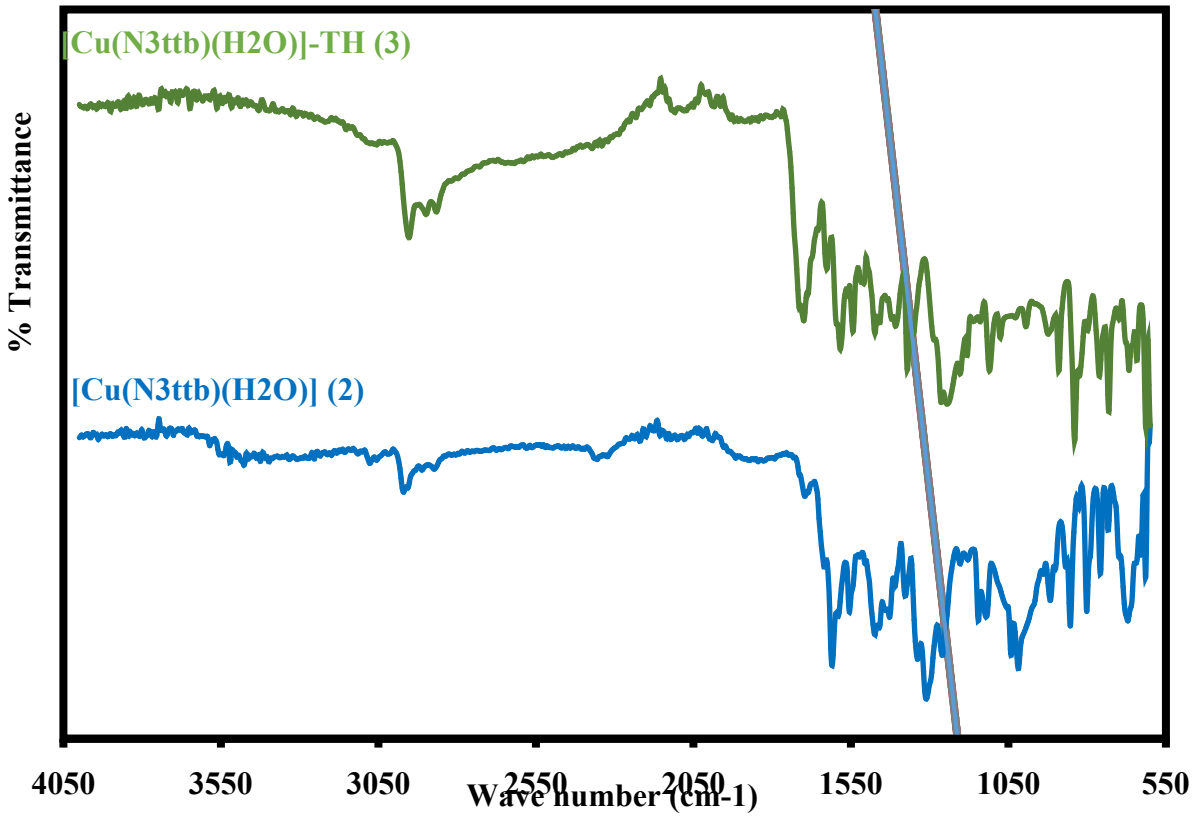

Figure S5: Comparison of the FT-IR spectra of as-synthesized (**2**) and thiol functionalized (**3**) Cu-MOFs

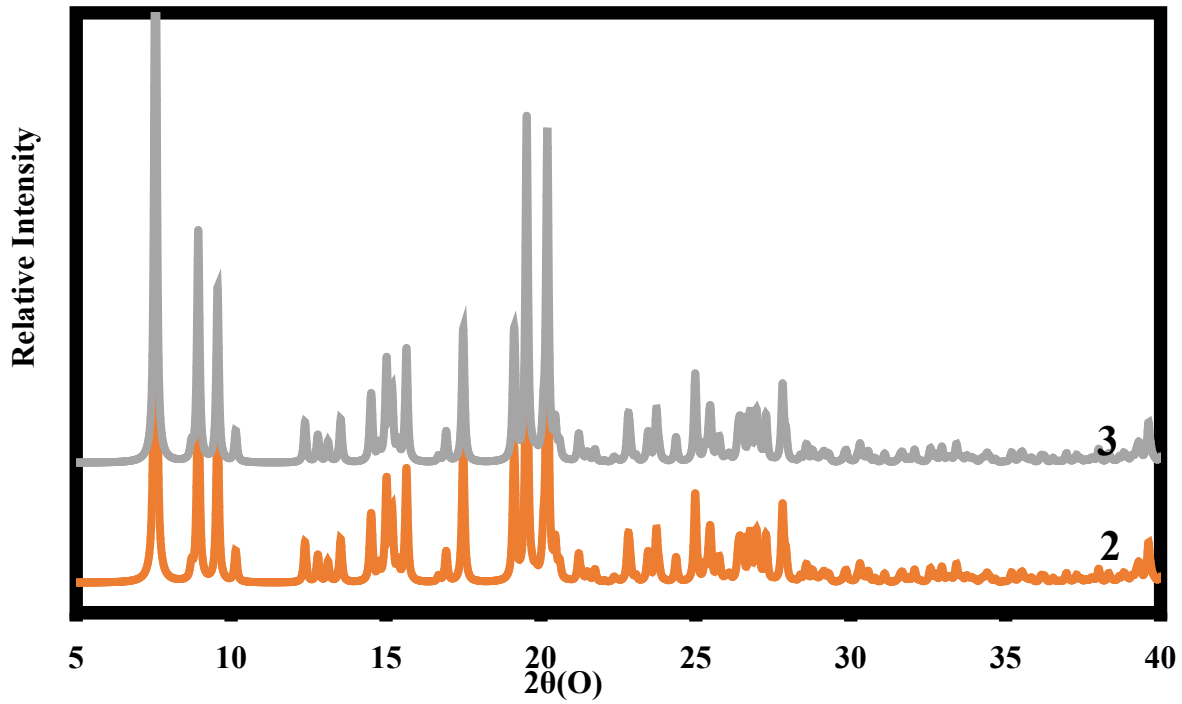

Figure S6: Comparison of the PXRD pattern of as-synthesized **2** and functionalized MOFs **3**

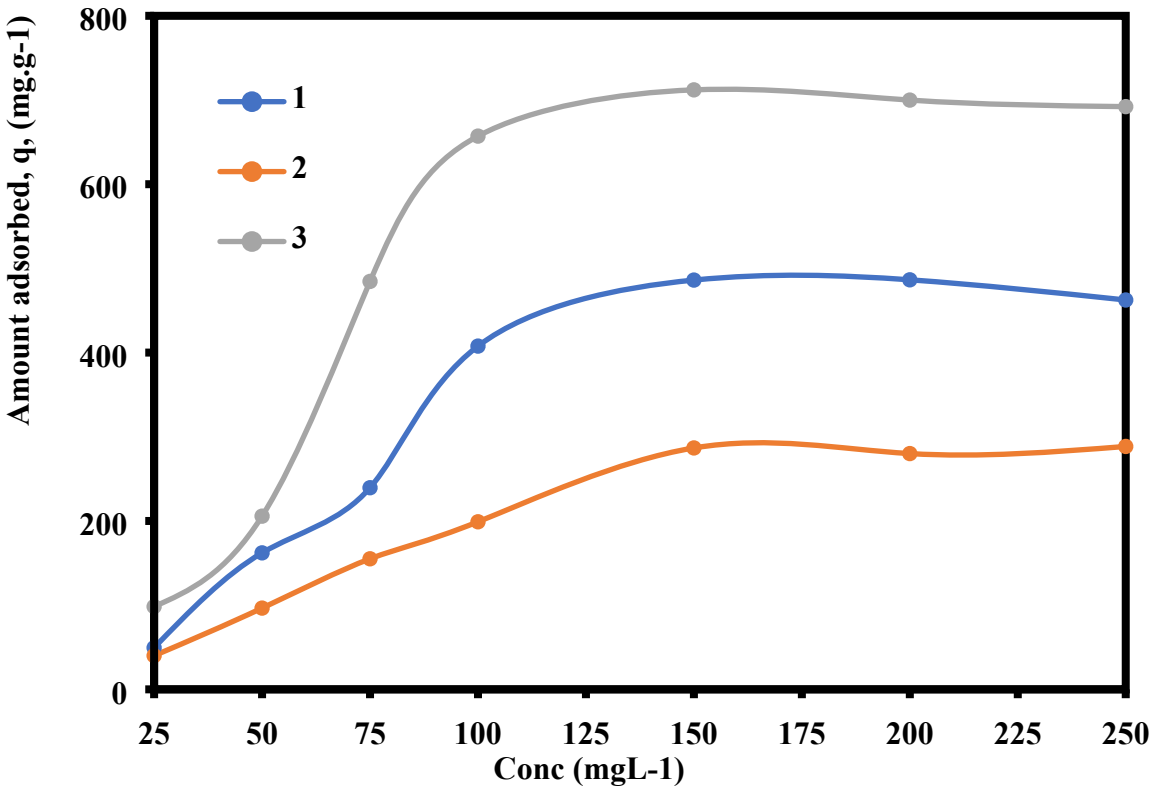

Figure S7: Effect of concentration on the adsorption of 2,4-D over **1**, **2** and **3**

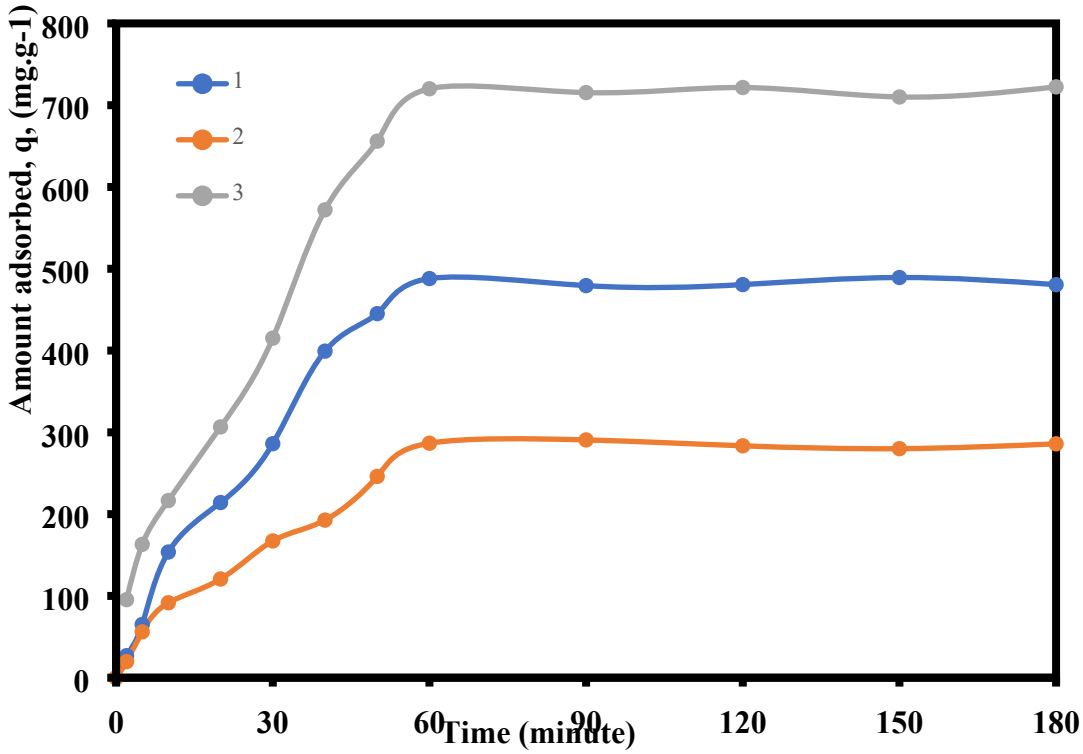

Figure S8: Effect of constant time on the adsorption of 2,4-D over **1**, **2** and **3**

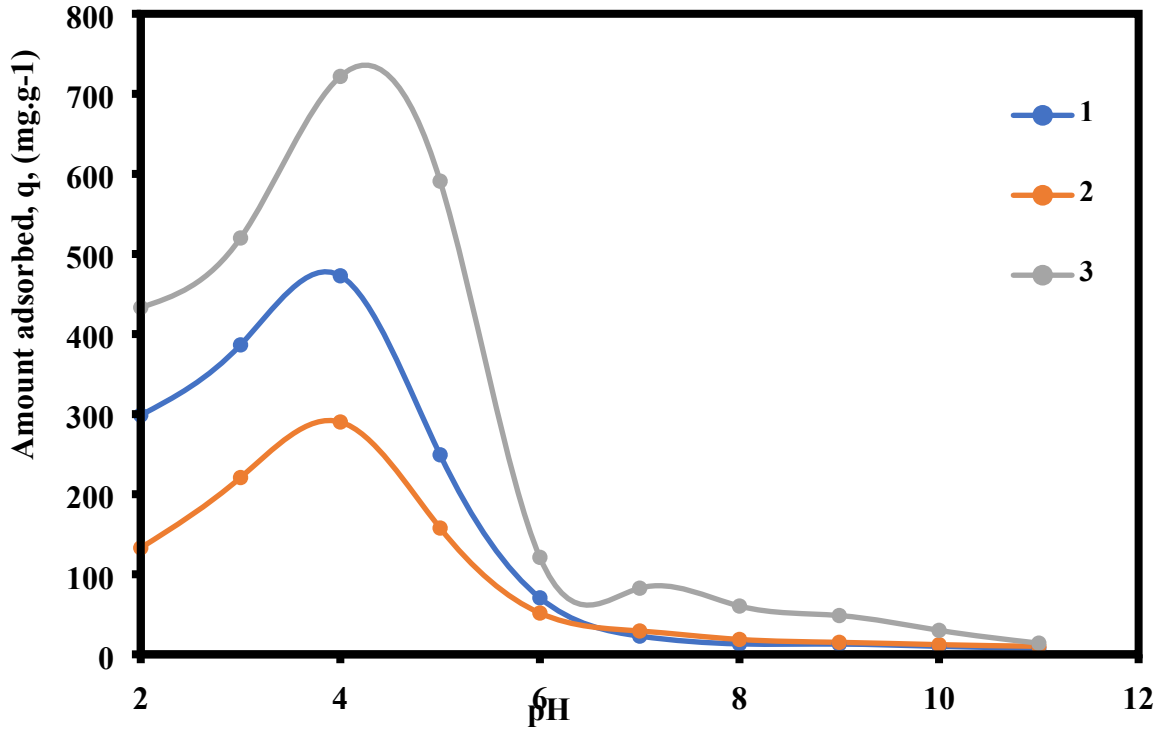

Figure S9: Effect of pH on the adsorption of 2,4-D over **1**, **2** and **3**

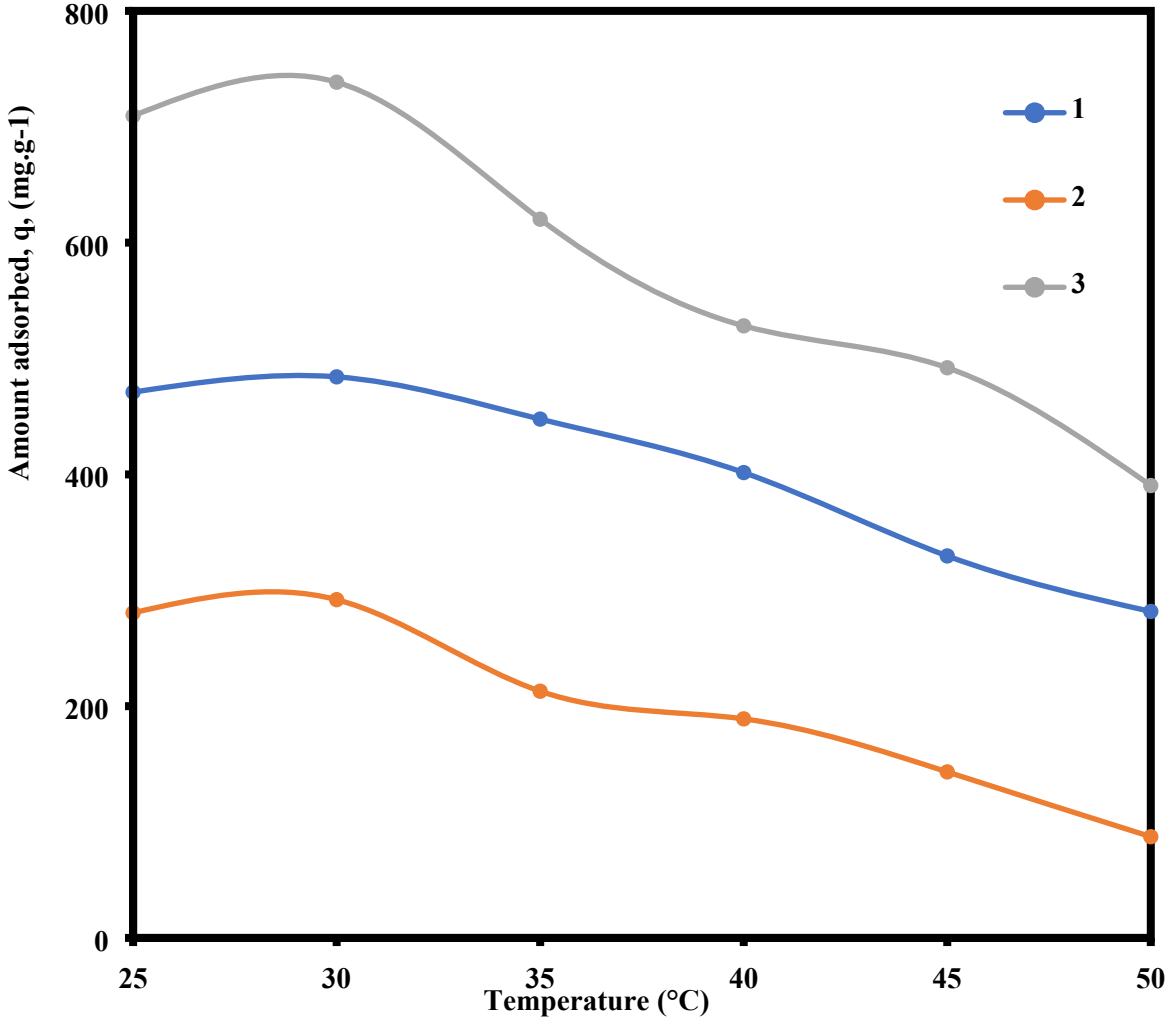

Figure S10: Effect of temperature on the adsorption of 2,4-D over **1**, **2** and **3**

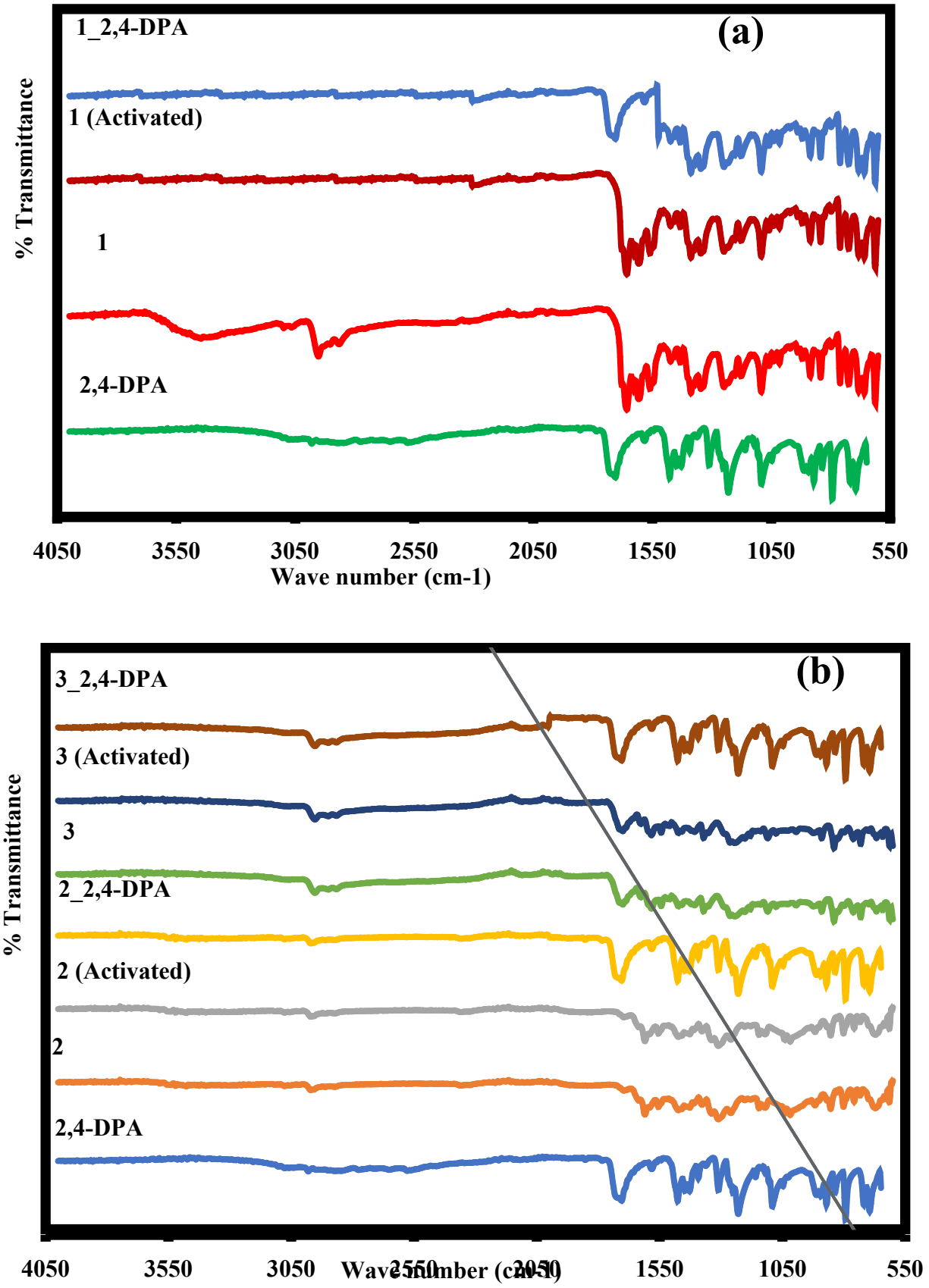

Figure S11: Infrared spectra of (a) **1** and (b) **2** & **3** before and after adsorption of 2,4-dichlorophenoxyacetic acid

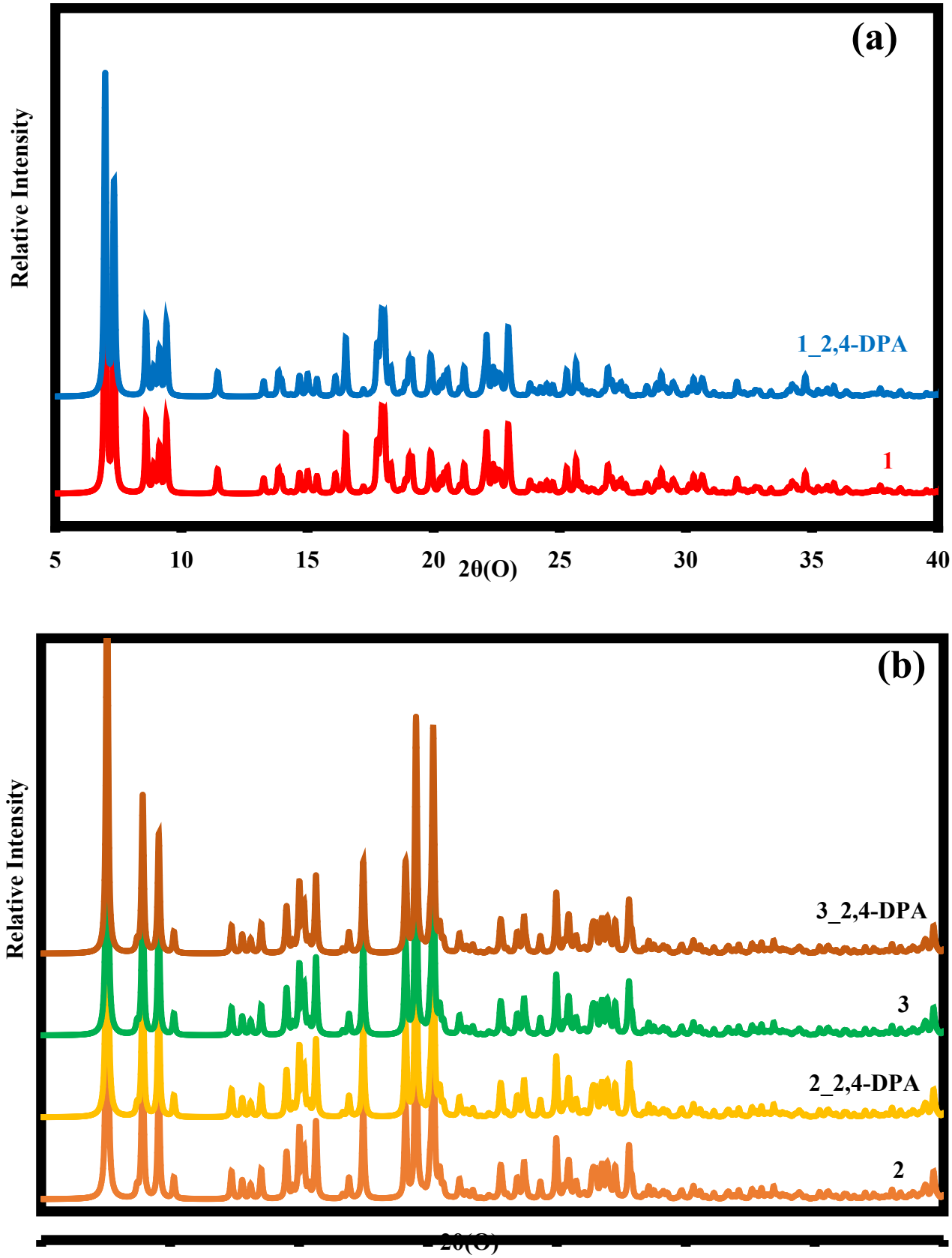

Figure S12: PXRD Pattern of (a) **1** and (b) **2** & **3** before and after adsorption of 2,4-dichlorophenoxyacetic acid

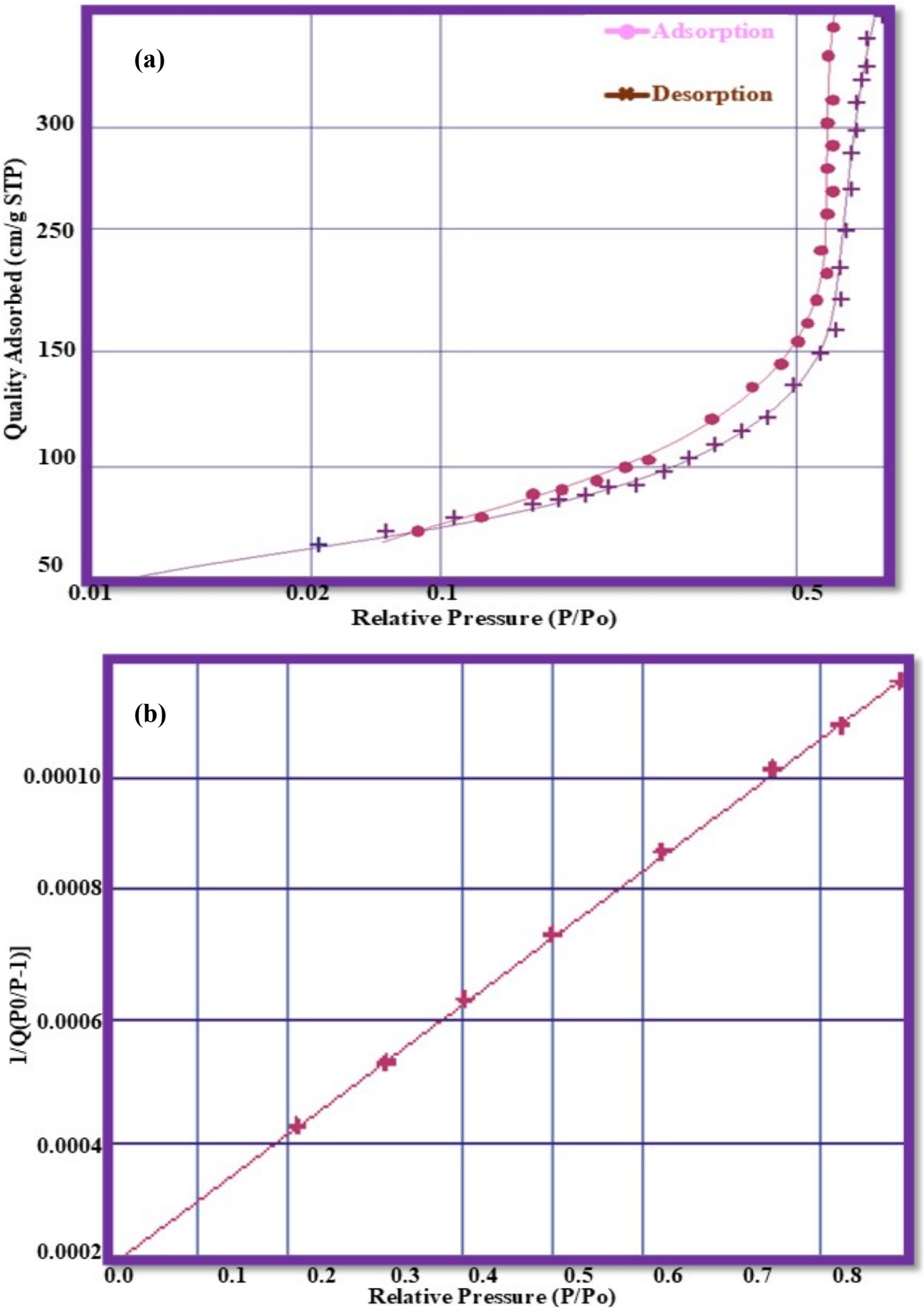

Figure S13: The graph of (a) N2 adsorption/desorption isotherms and (b) BET surface area plot of **1** before adsorption of 2,4-dichlorophenoxyacetic acid

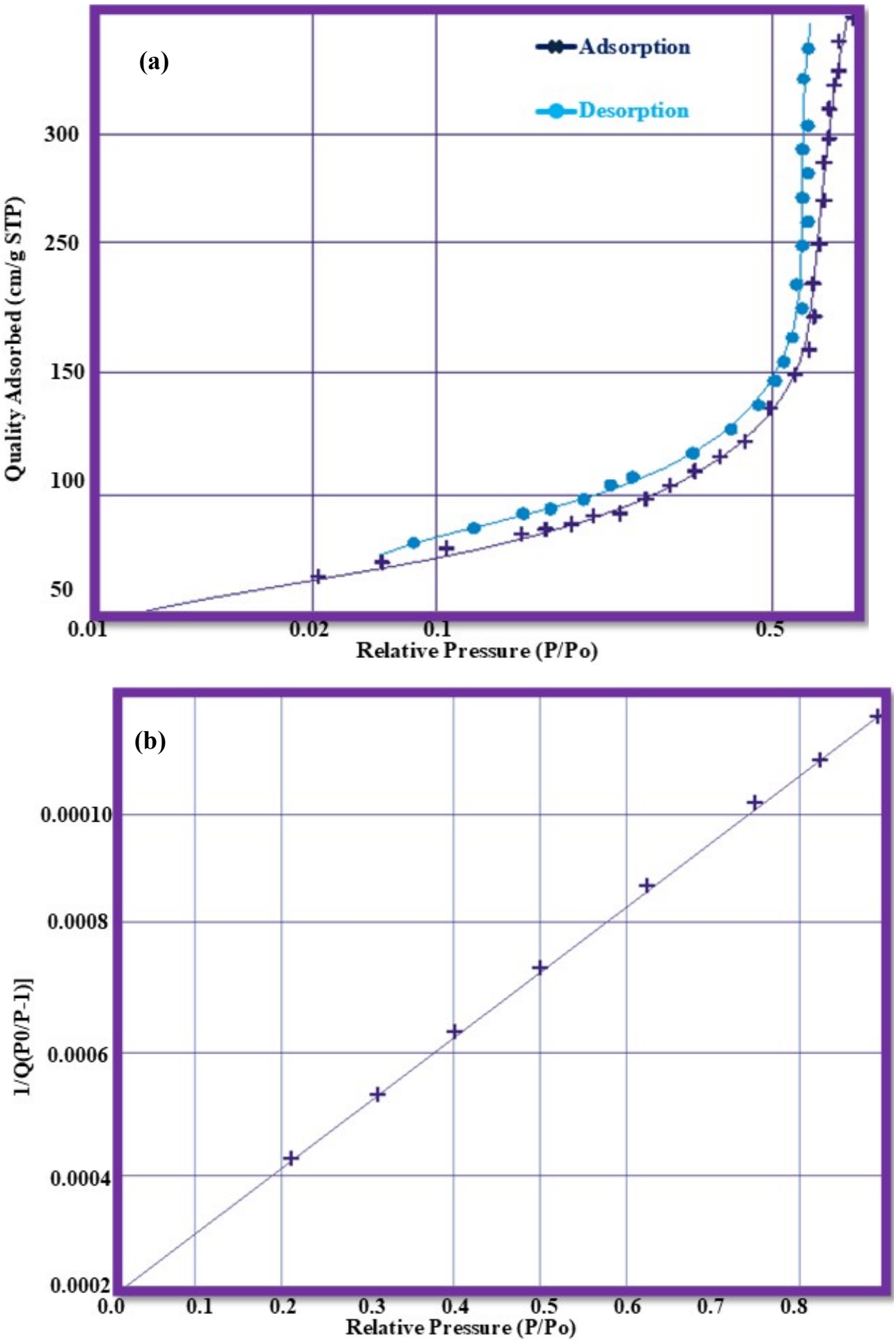

Figure S14: The graph of (a) N2 adsorption/desorption isotherms and (b) BET surface area plot of **2** before adsorption of 2,4-dichlorophenoxyacetic acid

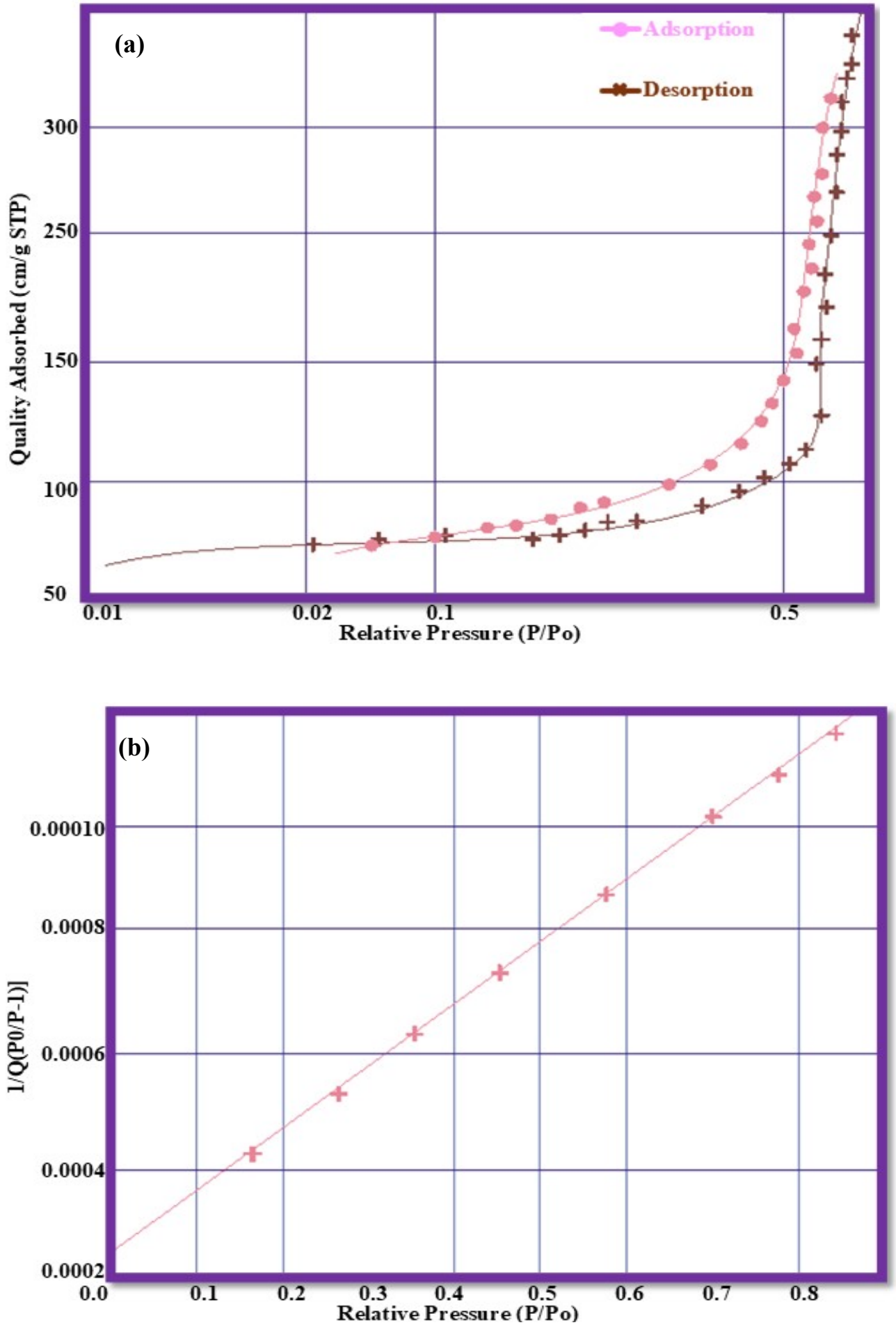

Figure S15: The graph of (a) N2 adsorption/desorption isotherms and (b) BET surface area plot of **3** before adsorption of 2,4-dichlorophenoxyacetic acid

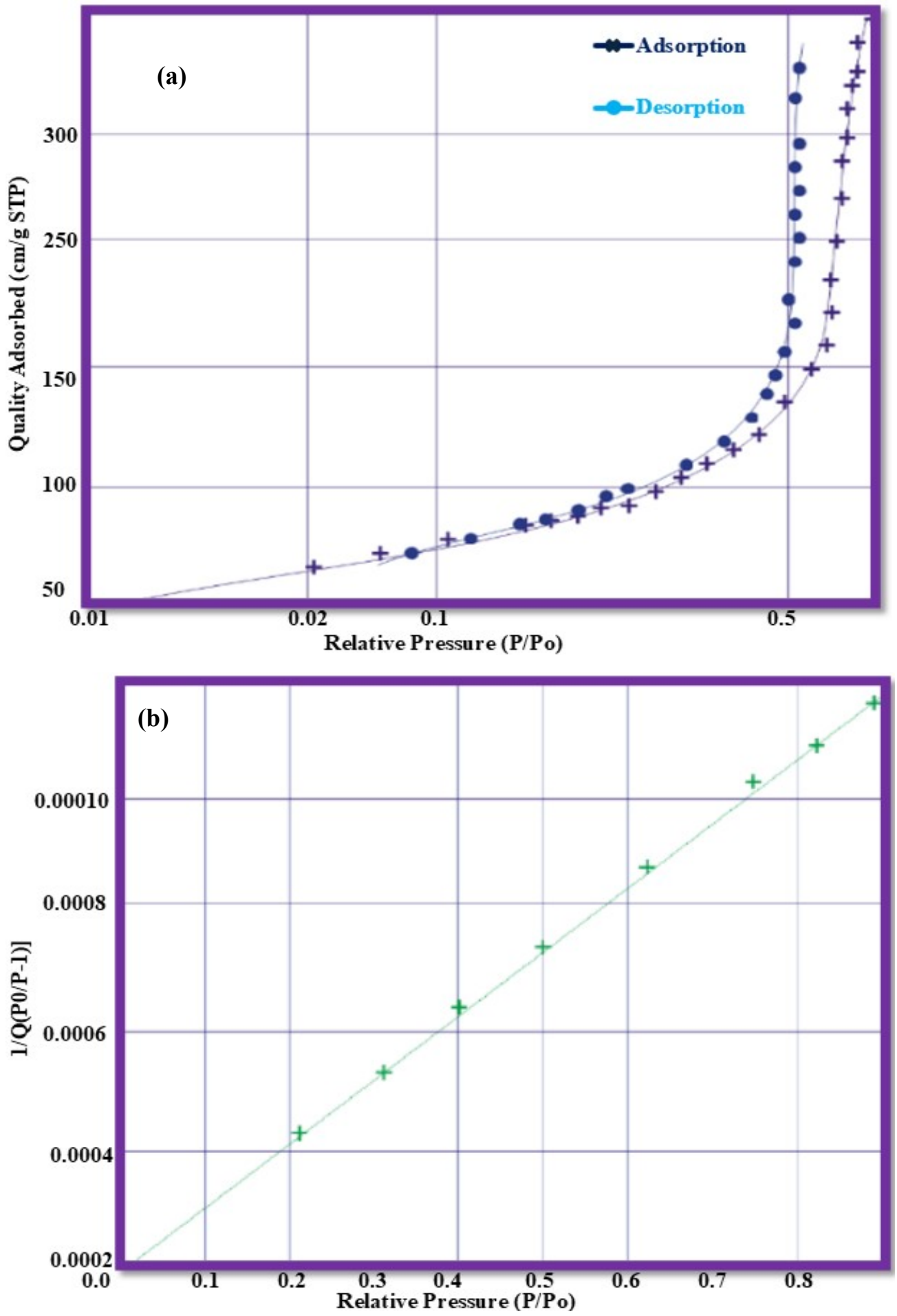

Figure S16: The graph of (a) N2 adsorption/desorption isotherms and (b) BET surface area plot of **1** after adsorption of 2,4-dichlorophenoxyacetic acid

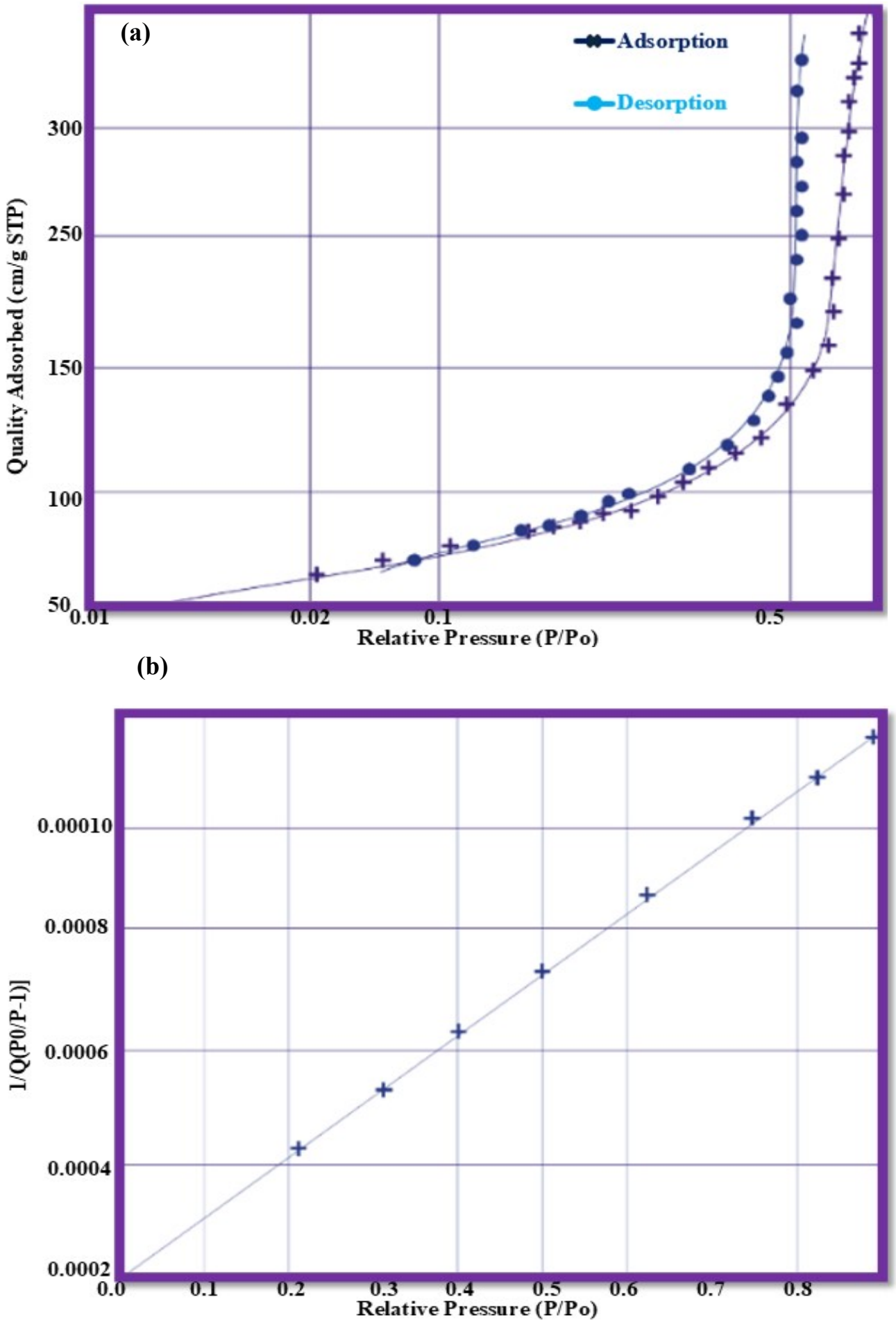

Figure S17: The graph of (a) N2 adsorption/desorption isotherms and (b) BET surface area plot of **2** after adsorption of 2,4-dichlorophenoxyacetic acid

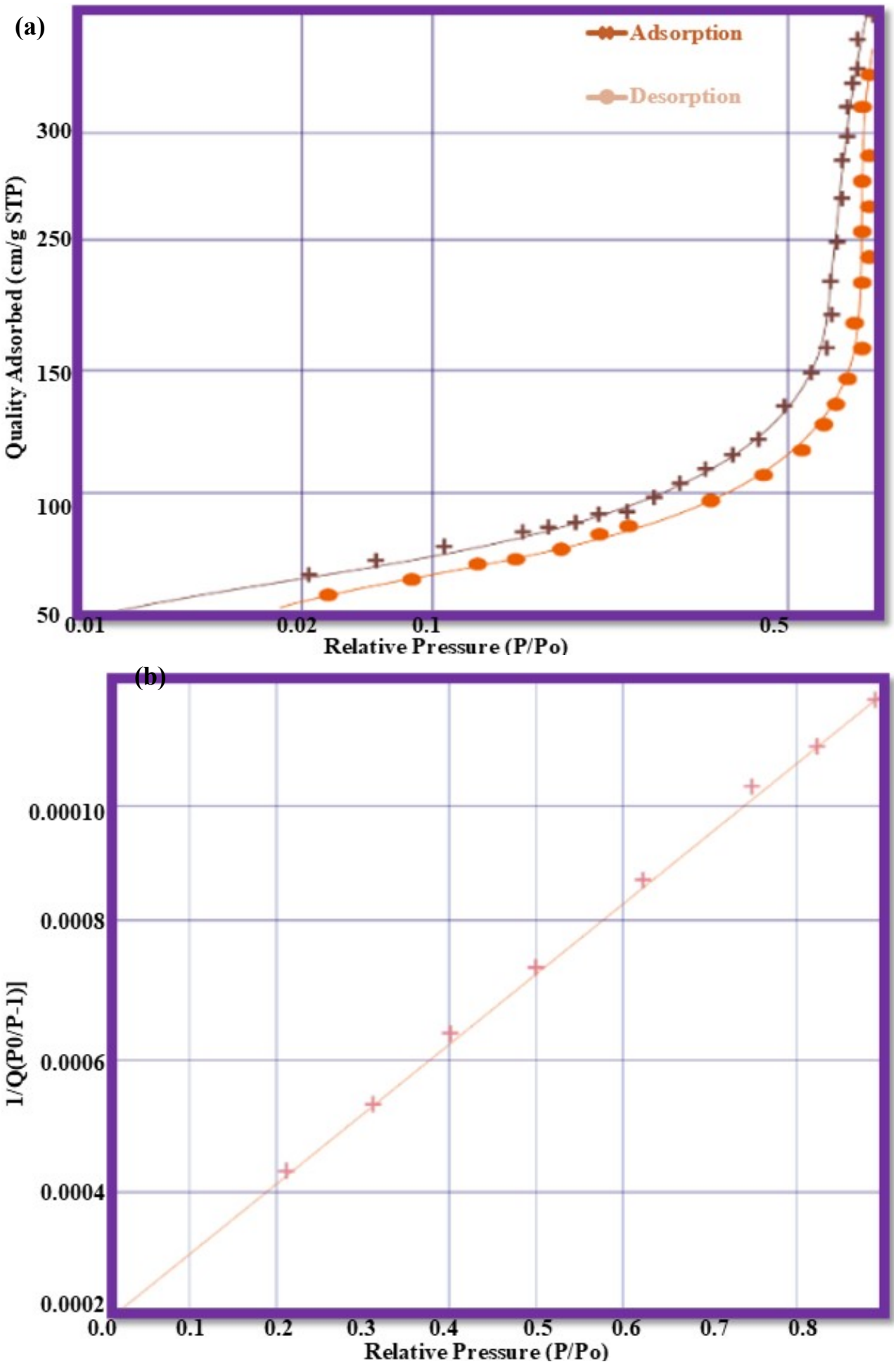

Figure S18: The graph of (a) N2 adsorption/desorption isotherms and (b) BET surface area plot of **3** after adsorption of 2,4-dichlorophenoxyacetic acid

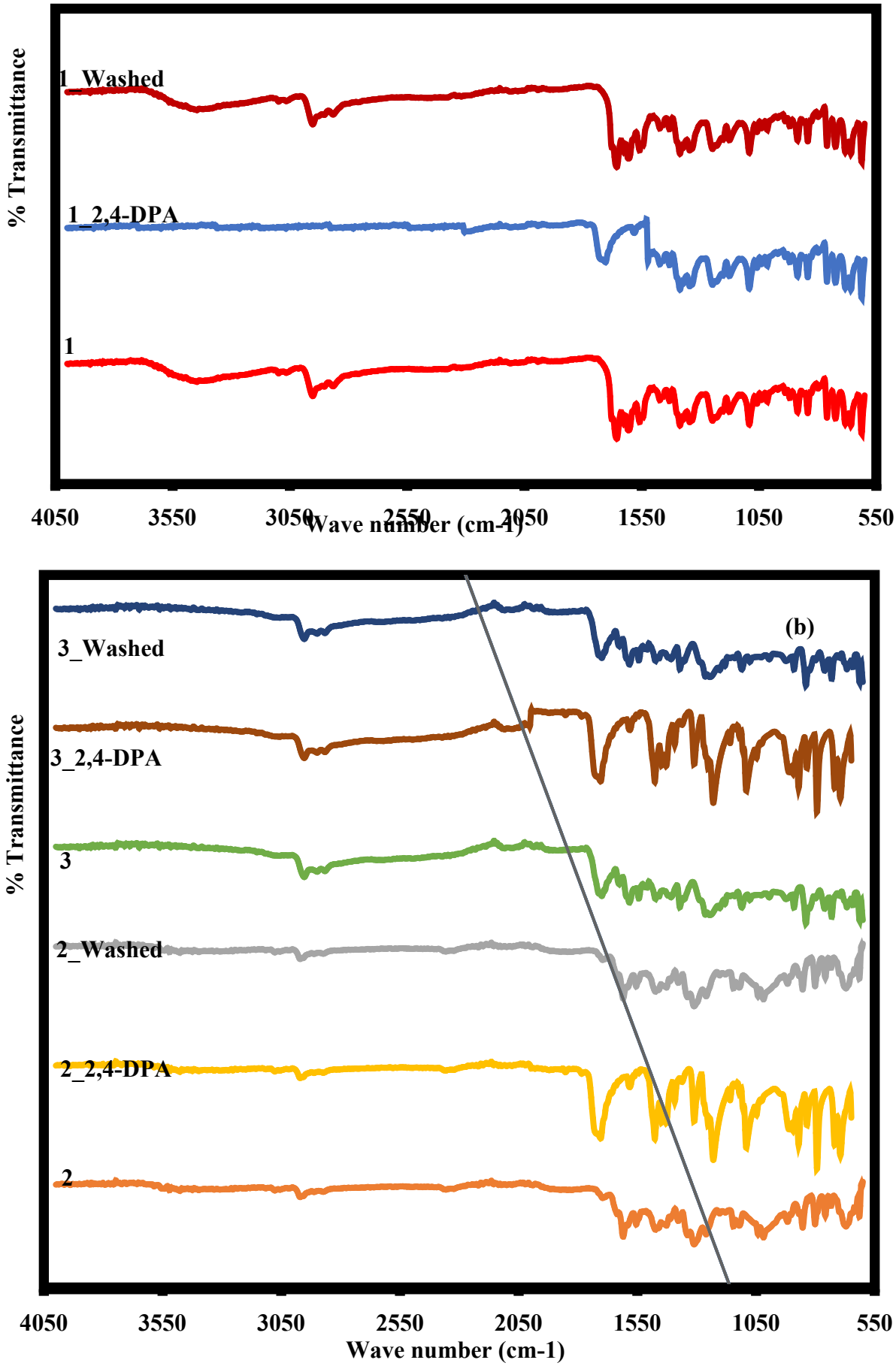

Figure S19: Infrared spectra to confirm reusability of (a) **1** and (b) **2** & **3** before and after adsorption of 2,4-dichlorophenoxyacetic acid

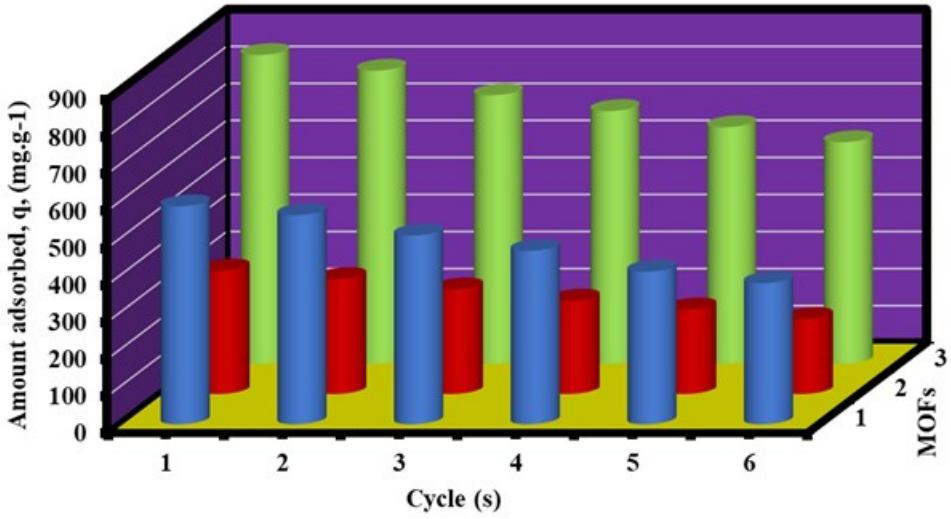

Figure S20: Reusability of **1**, **2** and **3** for Adsorption

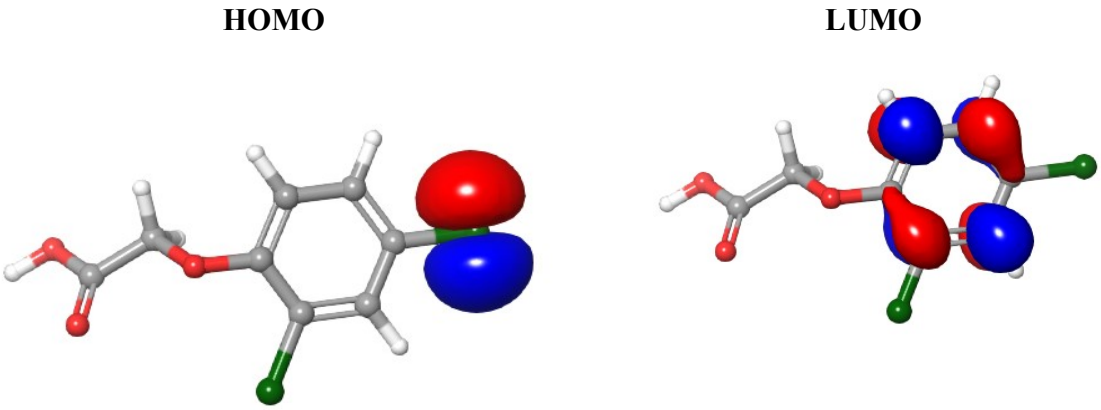

Figure S21: Frontier molecular orbitals of 2,4-dichlorophenoxyacetic acid where red is representing negative, and blue represents positive phases of the molecular frontier orbital wave function. Images generated by Maestro 13.6.

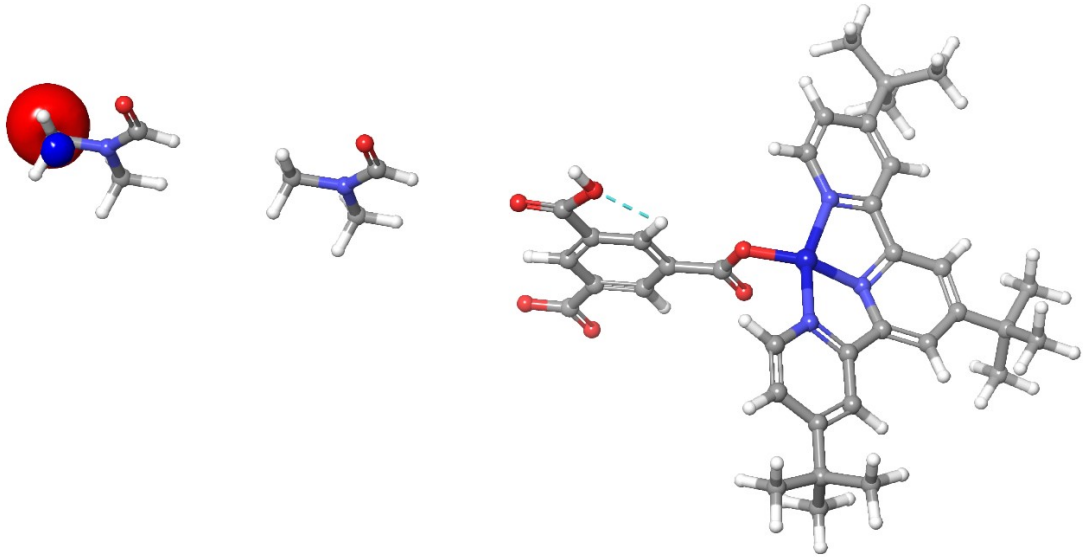

Figure S22: α HOMO orbitals of MOF1 where red is representing negative, and blue represents positive phases of the molecular frontier orbital wave function. Images generated by Maestro 13.6.

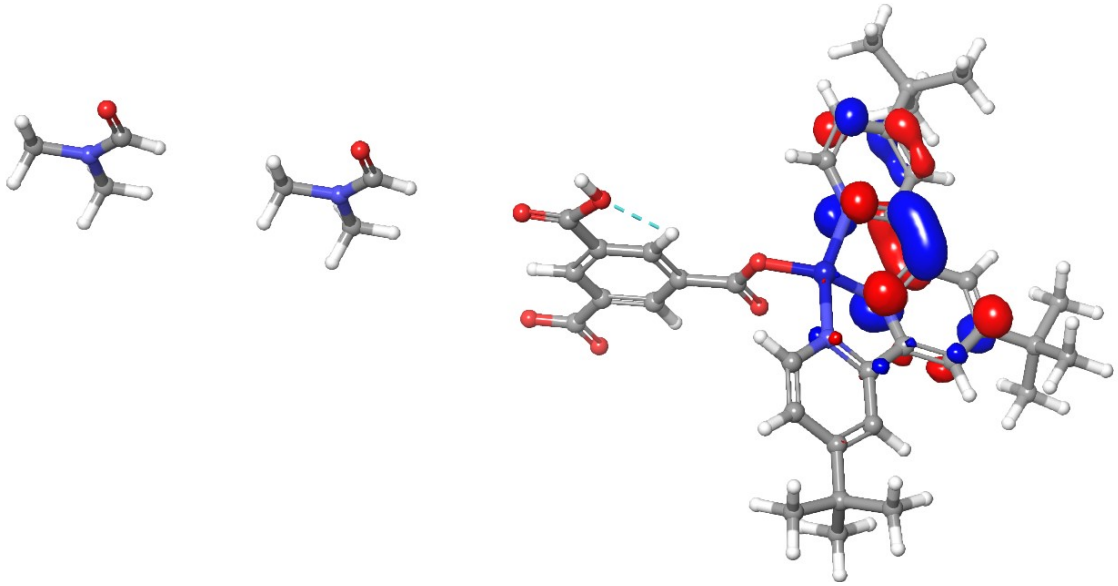

Figure S23: α LUMO orbitals of MOF1 where red is representing negative, and blue represents positive phases of the molecular frontier orbital wave function. Images generated by Maestro 13.6.

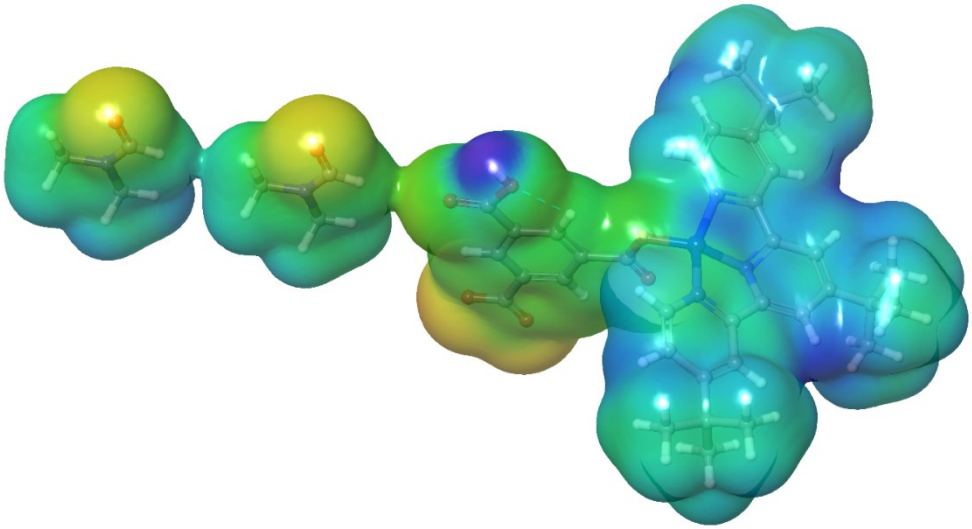

Figure S24: MESP of MOF1 mapped from volume. Images generated by Maestro 13.6.

aHOMO
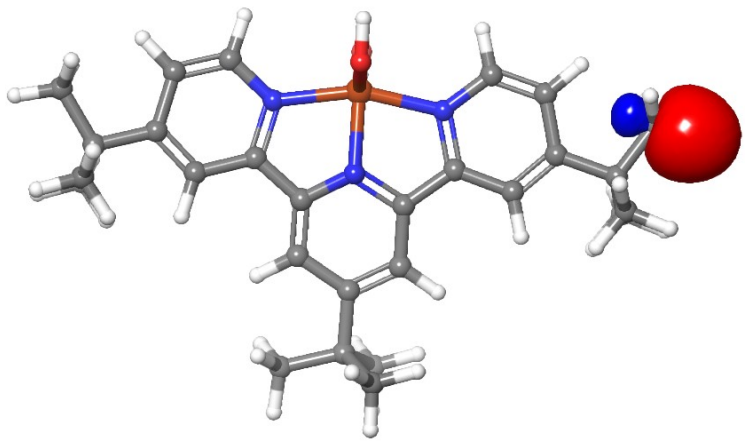

Figure S25: α HOMO orbitals of MOF2 where red is representing negative, and blue represents positive phases of the molecular frontier orbital wave function. Images generated by Maestro 13.6.

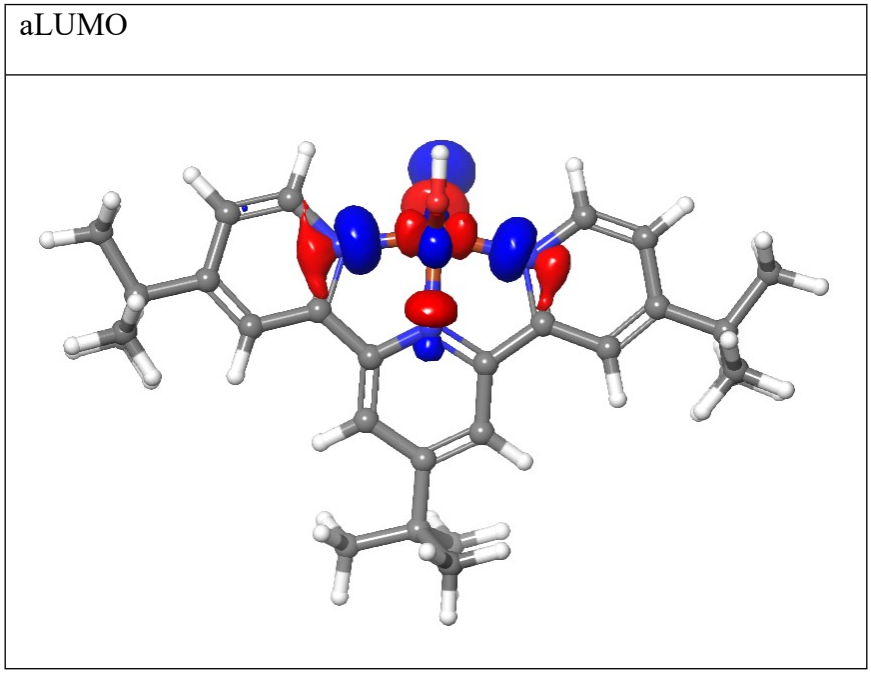

Figure S26: α LUMO orbitals of MOF2 where red is representing negative, and blue represents positive phases of the molecular frontier orbital wave function. Images generated by Maestro 13.6.

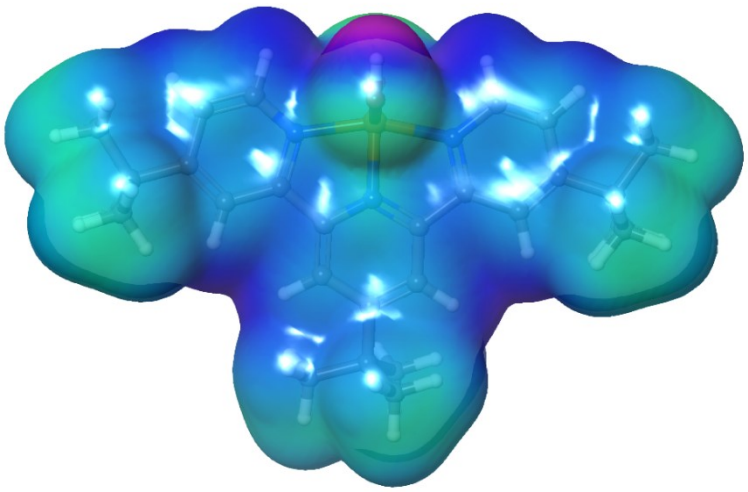

Figure S27: MESP of MOF2 mapped from volume. Images generated by Maestro 13.6.

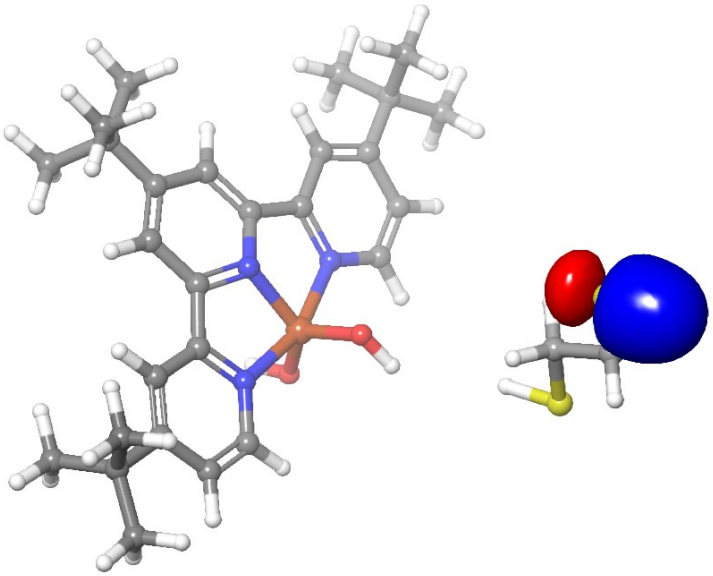

Figure S28: α HOMO orbitals of MOF3 where red is representing negative, and blue represents positive phases of the molecular frontier orbital wave function. Images generated by Maestro 13.6.

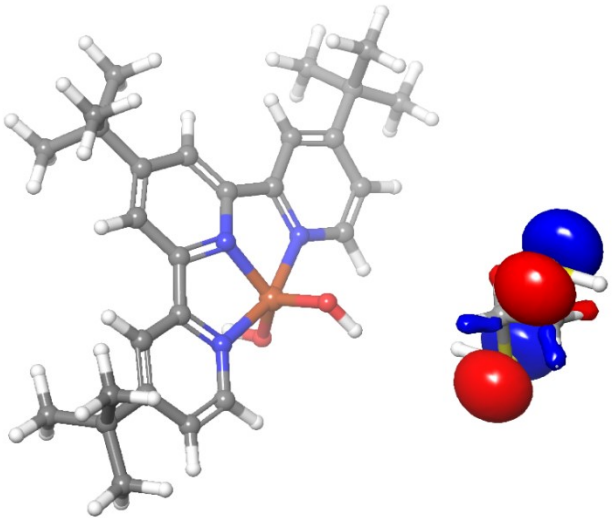

Figure S29: α LUMO orbitals of MOF3 where red is representing negative, and blue represents positive phases of the molecular frontier orbital wave function. Images generated by Maestro 13.6.

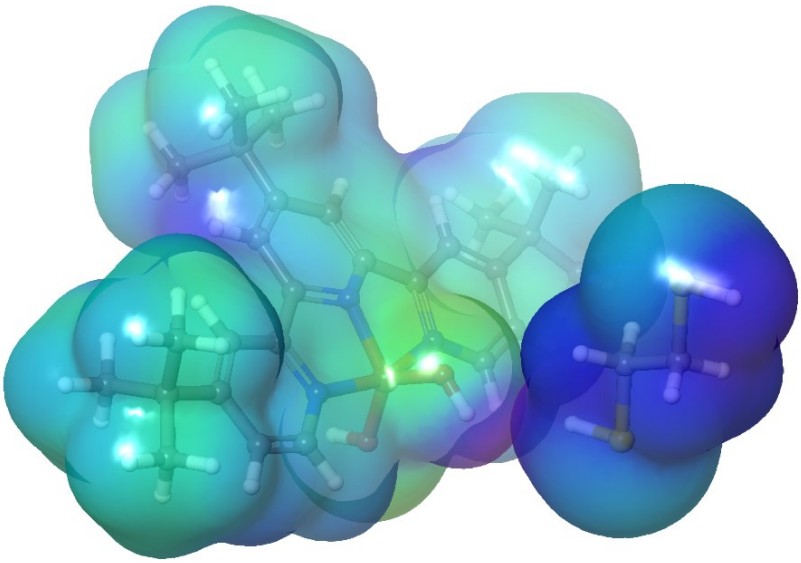

Figure S30: MESP of MOF3 mapped from volume. Images generated by Maestro 13.6

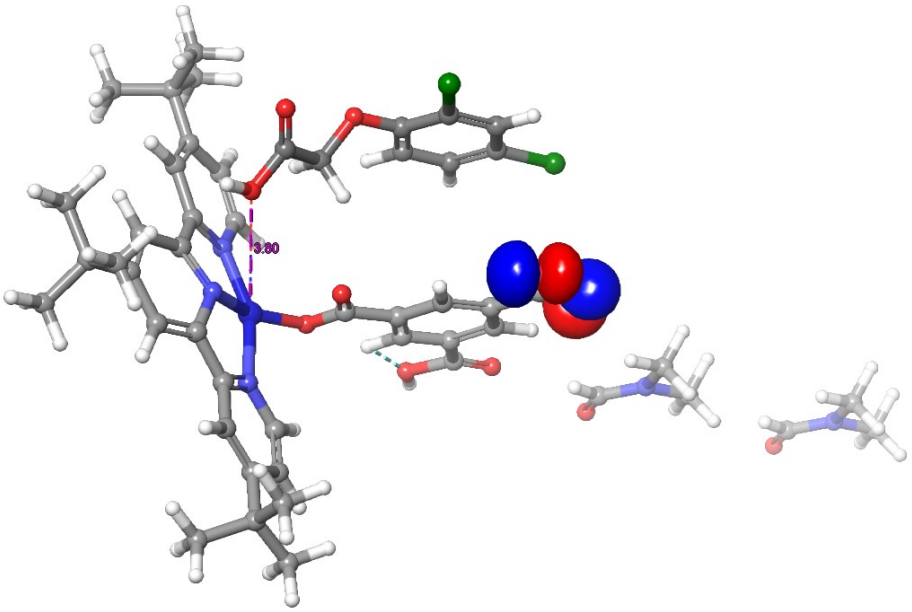

Figure S31*:* α-HOMO orbitals of MOF1@Herbicide where red is representing negative, and blue represents positive phases of the molecular frontier orbital wave function. Images generated by Maestro 13.6.

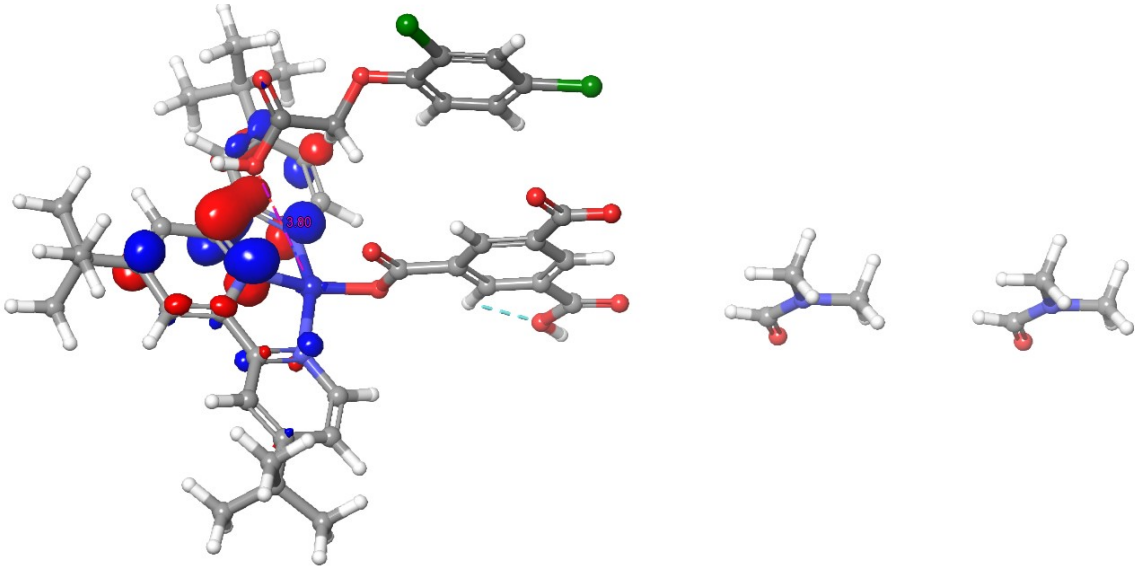

Figure S32*:* α-LUMO orbitals of MOF1@Herbicide where red is representing negative, and blue represents positive phases of the molecular frontier orbital wave function. Images generated by Maestro 13.6.

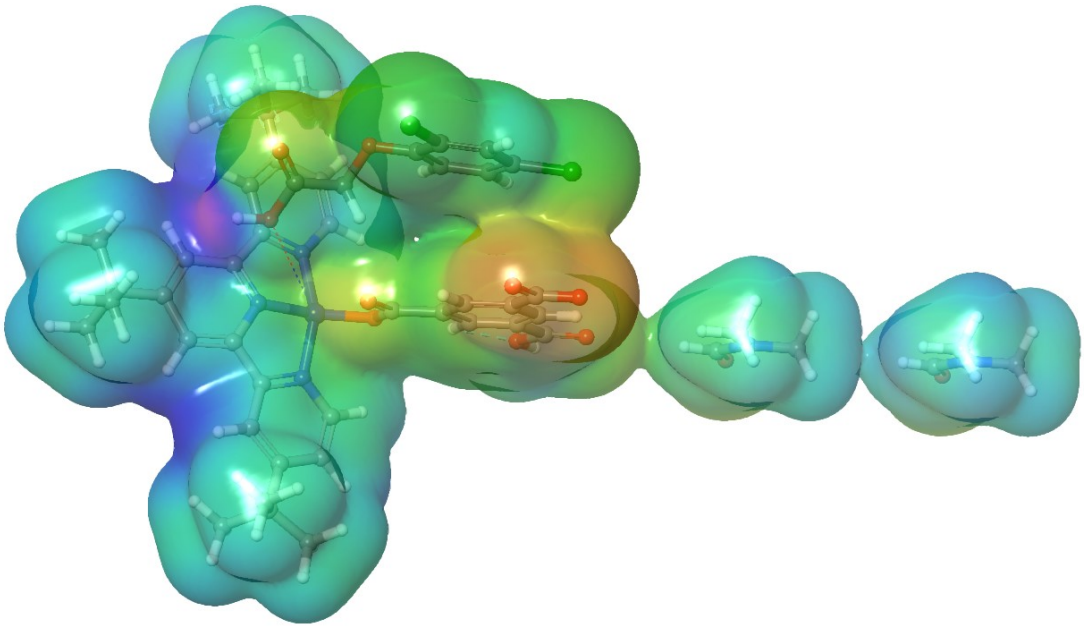

Figure 33: MESP of MOF1(3)@Herbicide mapped from volume. Images generated by Maestro 13.6

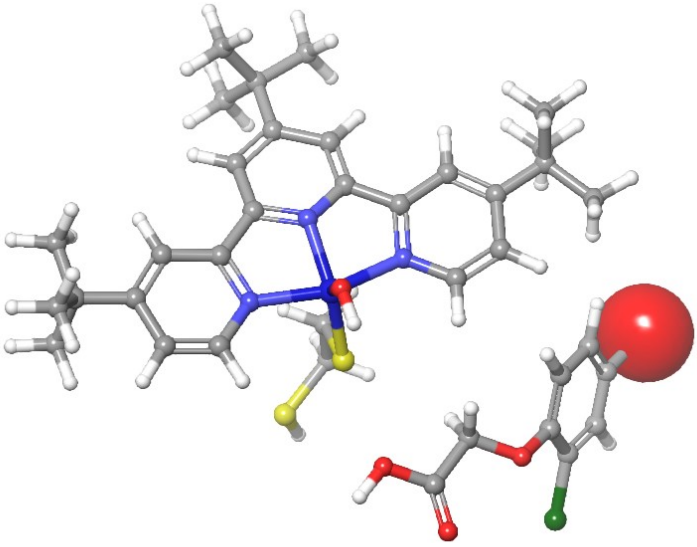

Figure S34: α-HOMO orbitals of MOF3@Herbicide where red is representing negative, and blue represents positive phases of the molecular frontier orbital wave function. Images generated by Maestro 13.6.

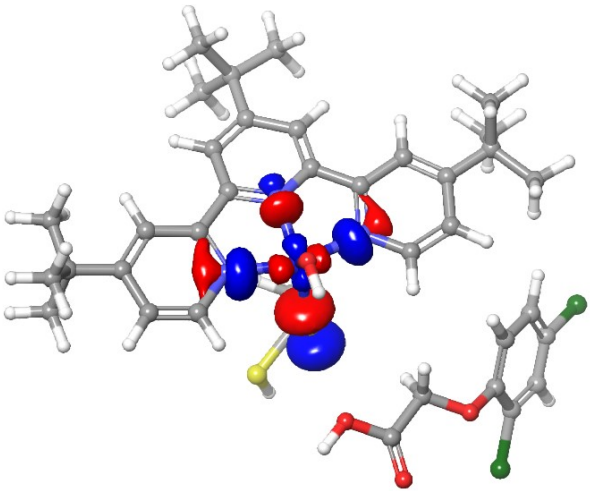

Figure S35: α-LUMO orbitals of MOF3@Herbicide where red is representing negative, and blue represents positive phases of the molecular frontier orbital wave function. Images generated by Maestro 13.6.

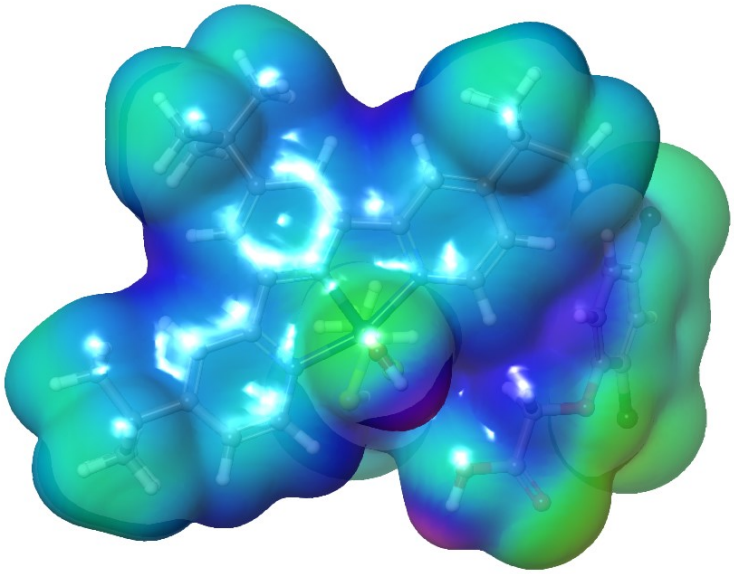

Figure S36: MESP of MOF2(3)@Herbicide mapped from volume. Images generated by Maestro 13.6

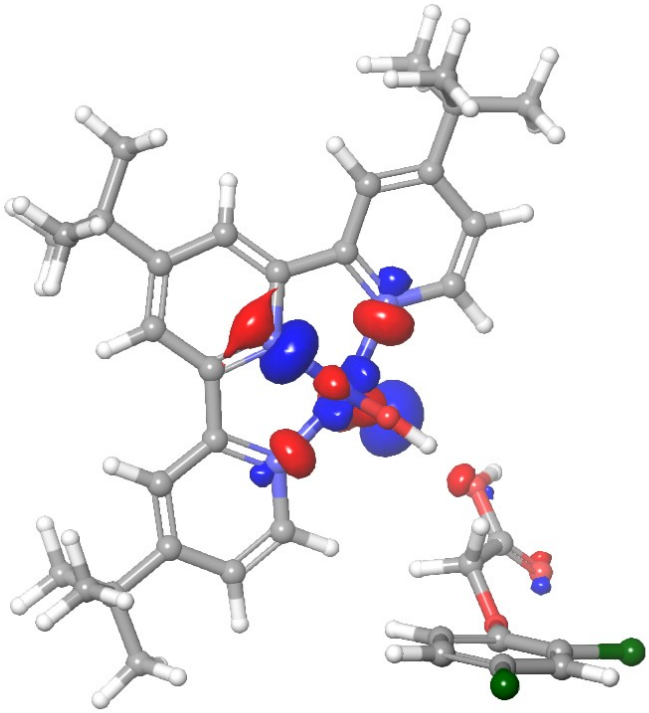

Figure S37: α-HOMO orbitals of MOF2@Herbicide where red is representing negative, and blue represents positive phases of the molecular frontier orbital wave function. Images generated by Maestro 13.6.

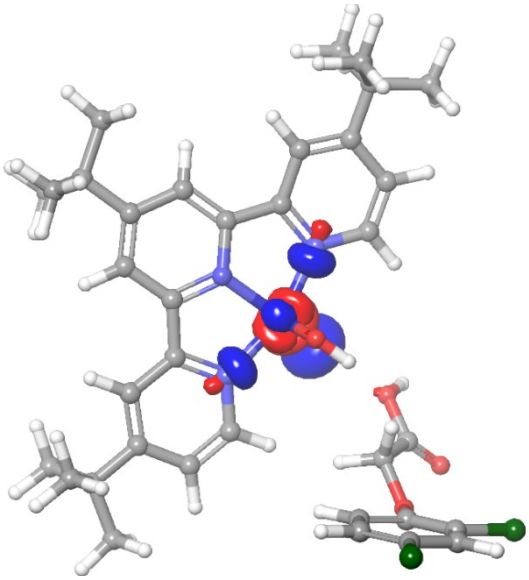

Figure S38: α LUMO orbitals of MOF2@Herbicide where red is representing negative, and blue represents positive phases of the molecular frontier orbital wave function. Images generated by Maestro 13.6.

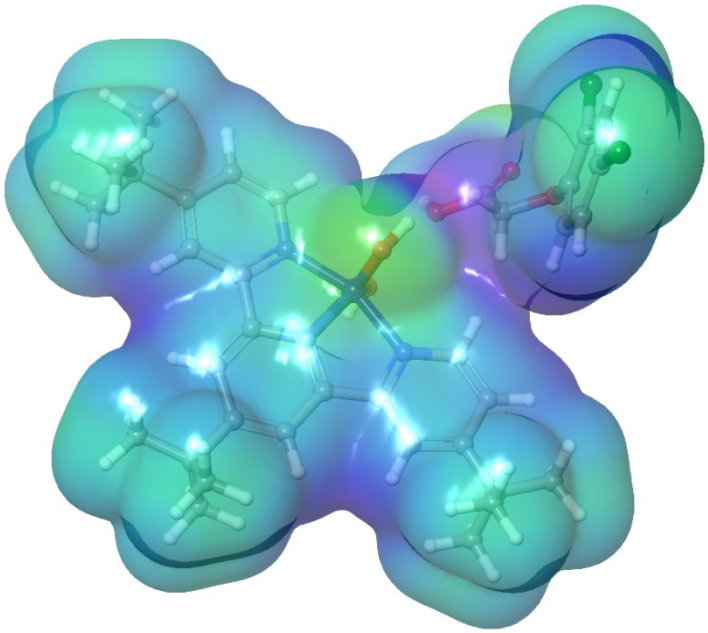

Figure S39: MESP of MOF3@Herbicide mapped from volume. Images generated by Maestro 13.6

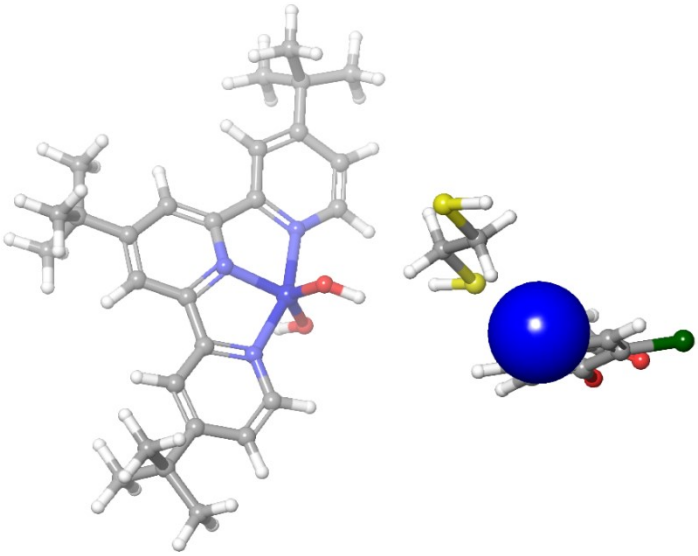

Figure S40: α HOMO orbitals of MOF3@Herbicide 2 where red is representing negative, and blue represents positive phases of the molecular frontier orbital wave function. Images generated by Maestro 13.6.

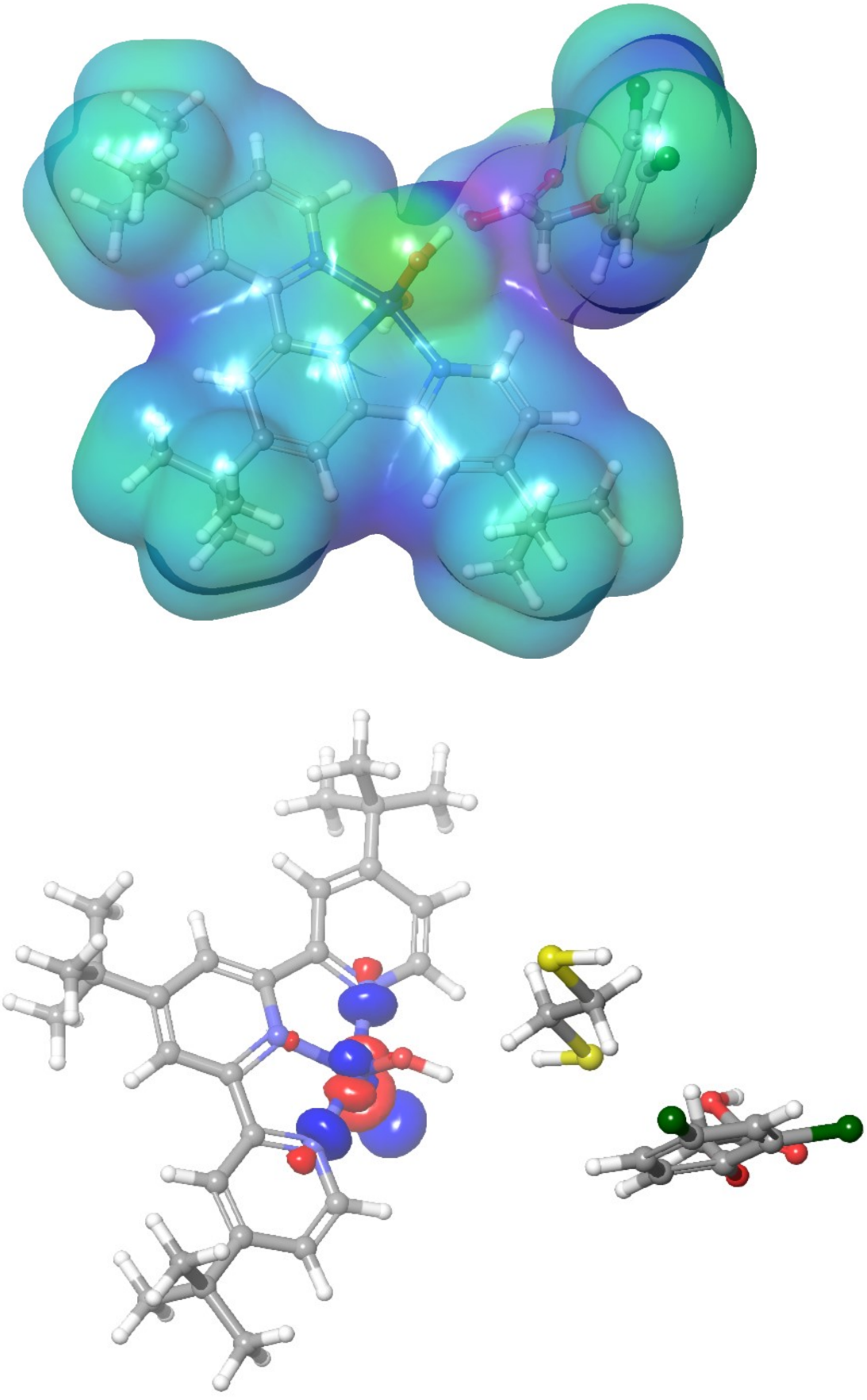

Figure S41*:* α LUMO orbitals of MOF3@Herbicide 2 where red is representing negative, and blue represents positive phases of the molecular frontier orbital wave function. Images generated by Maestro 13.6.

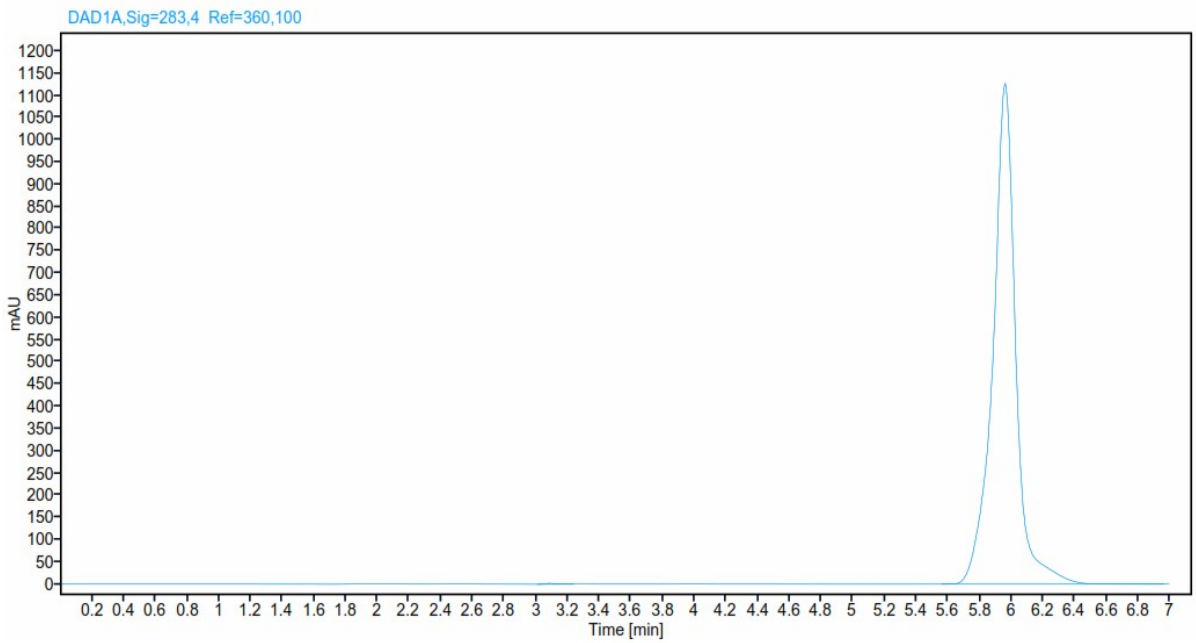

Figure S42: Chromatogram of 2,4-Dhlorophenoxyacetic acid (150 mgL^{-1} before adsorption)

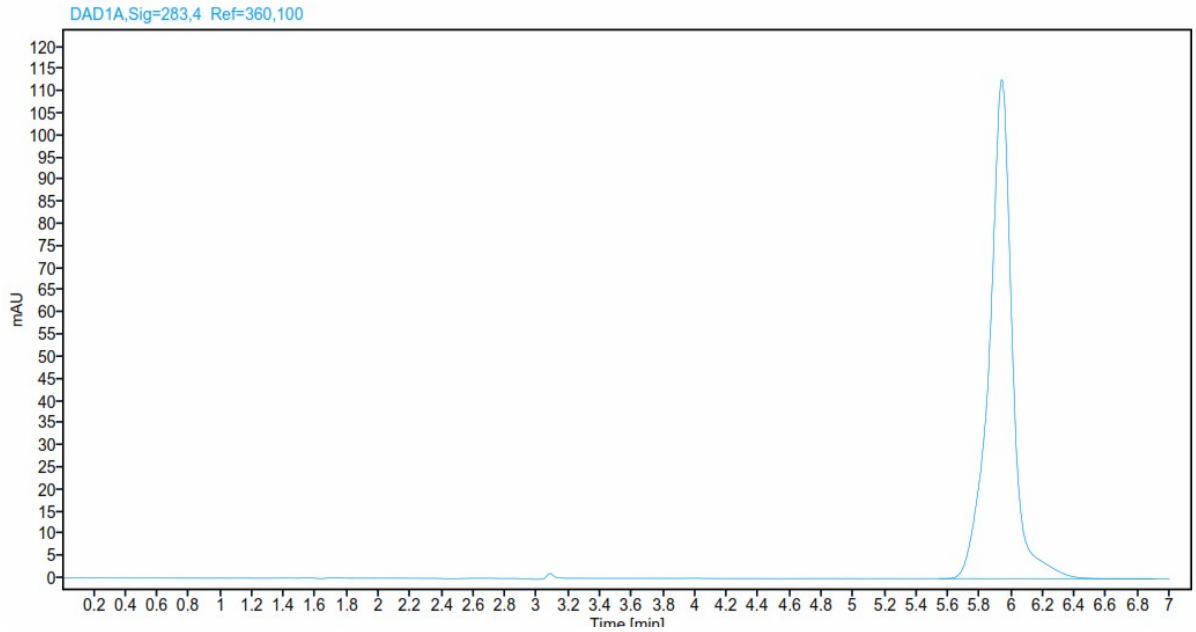

Figure S43: Chromatogram of 2,4-Dhlorophenoxyacetic acid after removal over **1**.

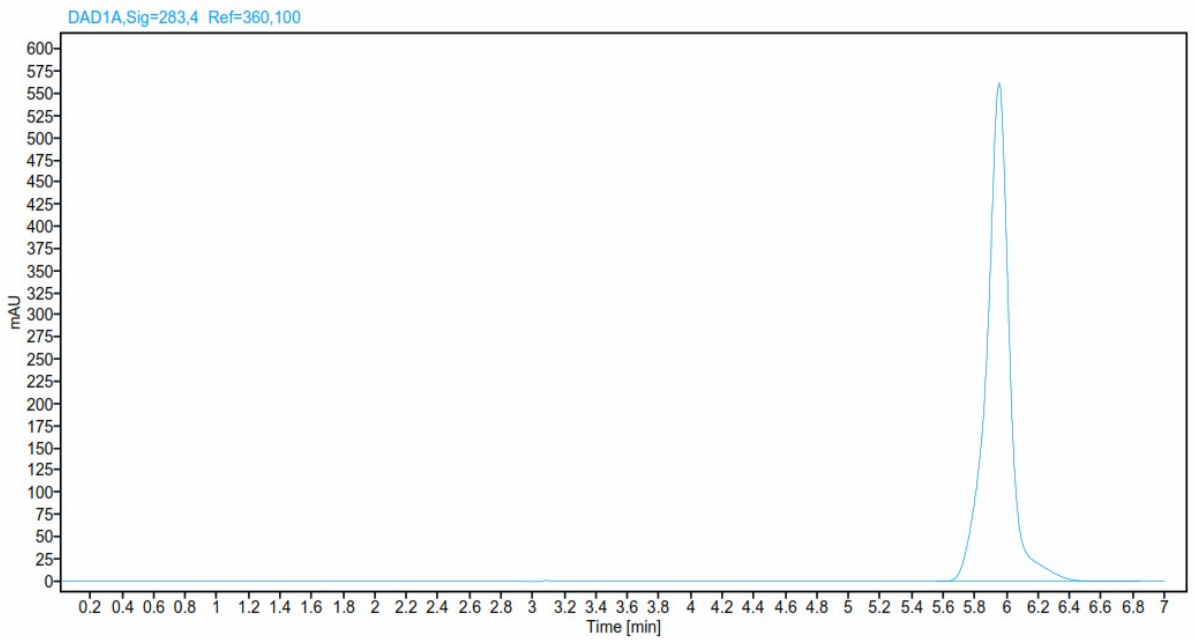

Figure S44: Chromatogram of 2,4-Dhlorophenoxyacetic acid after removal over **2**.

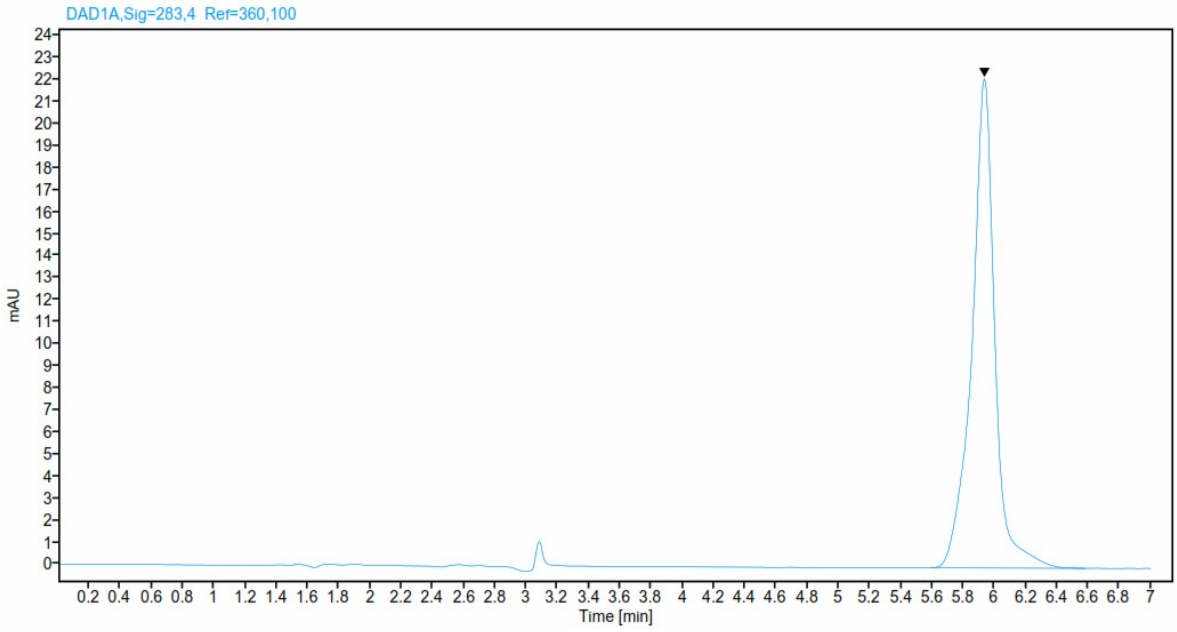

Figure S45: Chromatogram of 2,4-Dhlorophenoxyacetic acid after removal over **3**.

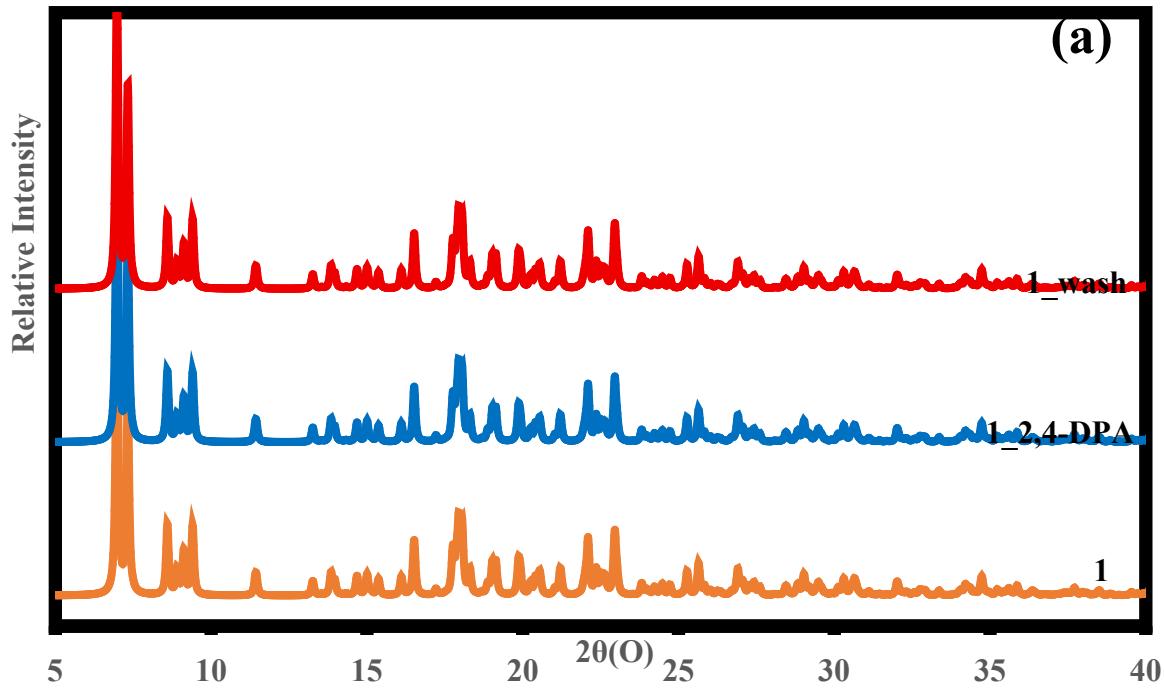
(a)
Relative Intensity
1_wash
1_2,4-DPA
1
5
10
15
20
2θ(O)
25
30
35
40

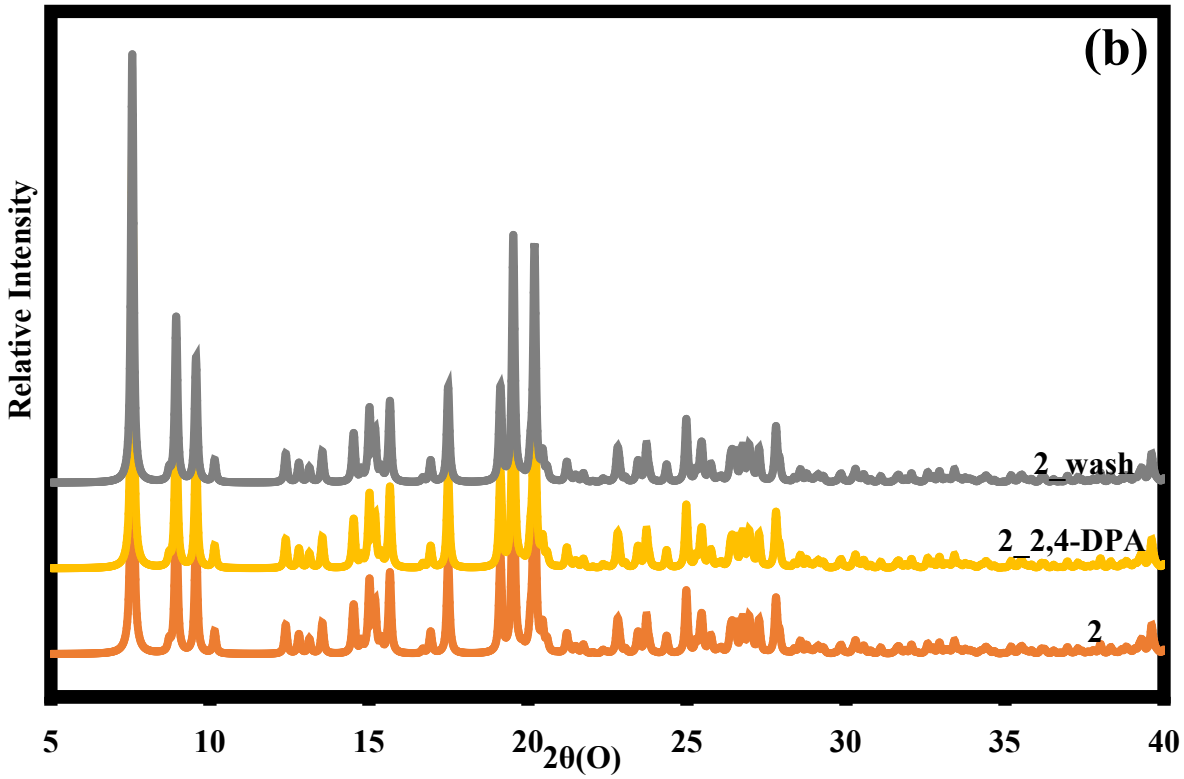
(b)
Relative Intensity
2_wash
2_2,4-DPA
2
5
10
15
20
2θ(O)
25
30
35
40

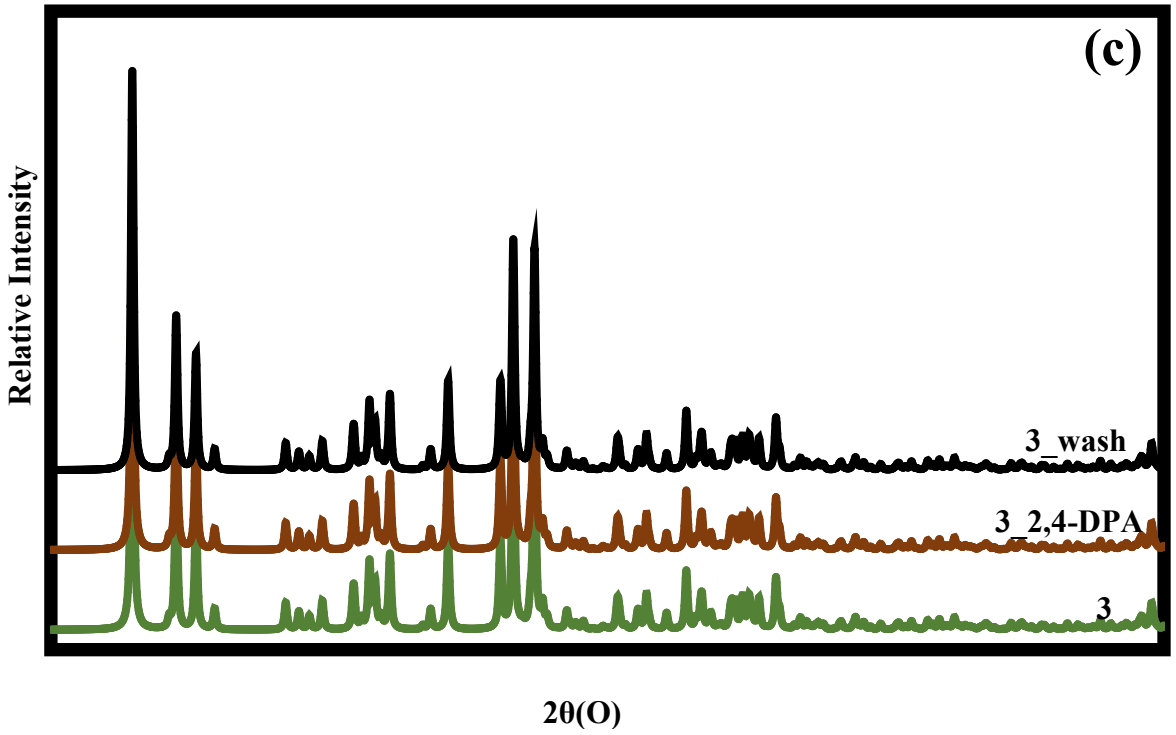

Figure S46: PXRD Pattern to confirm reusability of (a) **1,** (b) **2** and (c) **3** before and after adsorption of 2,4-dichlorophenoxyacetic acid

Table S1: Intramolecular hydrogen bonding

D----H….A	**D⁻---H (Å)**	**H….A (Å)**	**D ….A (Å)**	**D⁻---H….A** Symmetry operation for **-A**
O5---- H5…O4	0.84	1.716	2.549	1-x, 1-y, -z
C14---H14…..O8	0.949	2.569	3.518	x, -1+y, z
C24---H24C…O7	0.960	2.597	3.501	-1+ x, y, z
C39----H39…O5	0.960	2.474	3.190	1 – x, 1 -y, -z
C4------H4….O2	0.960	2.436	3.067	-1 + x, y, z
C7------H7….O2	0.960	2.574	3.366	-1 + x, y, z
C9------H9….O7	0.961	2.530	3.444	X, 1 + y, z
C28---H28a….O8	0.976	2.569	3.633	x, -1+y, z
C30---H30a.....O8	0.979	2.536	3.361	x, -1+y, z
C32----H32….O8	0.950	2.666	3.367	x, -1+y, z
C33---H33b.O1	0.98	2.53	3.270	1 - x, 1 – y, 1 – z.
C9-----H9…...O7	0.961	2.530	3.449	x, 1+y, z
C33---H33c….O1	0.961	2.525	3.270	X, y, z
C17---H17a….O2	0/961	2.662	3.566	-1 + x, y, z
C12----H12….O7	0.945	2.603	3.524	X, 1 +y, z

Table S2: adsorption isotherm experimental data for Compound **1**

C0	Ce (mg/L)			qe (mg/g)			Mean qe	SD
(mg/L)	rep 1	rep 2	rep 3	rep 1	rep 2	rep 3	(mg/g)	(mg/g)
25.000	20.054	19.901	20.162	49.460	50.990	48.380	49.610	1.311
50.000	33.788	34.297	34.003	162.120	157.030	159.970	159.707	2.555
75.000	51.050	52.028	51.815	239.500	229.720	231.850	233.690	5.143
100.000	59.229	60.914	61.006	407.710	390.860	389.940	396.170	10.005
150.000	101.387	102.108	101.829	486.130	478.920	481.710	482.253	3.636
200.000	151.357	152.903	152.028	486.430	470.970	479.720	479.040	7.752
250.000	203.754	202.582	201.042	462.460	474.180	489.580	475.407	13.602

Table S3: adsorption isotherm experimental data for Compound **2**

C0	Ce (mg/L)			qe (mg/g)			Mean qe	SD
(mg/L)	rep 1	rep 2	rep 3	rep 1	rep 2	rep 3	(mg/g)	(mg/g)
25.000	20.998	20.836	20.906	40.020	41.640	40.940	40.867	0.812
50.000	40.349	40.196	39.729	96.510	98.040	102.710	99.087	3.230
75.000	59.492	60.027	59.814	155.080	149.730	151.860	152.223	2.693
100.000	80.097	81.148	79.999	199.030	188.520	200.010	195.853	6.370
150.000	121.326	122.205	121.073	286.740	277.950	289.270	284.653	5.941
200.000	171.995	172.027	171.736	280.050	279.730	282.640	280.807	1.596
250.000	221.148	225.326	222.286	288.520	246.740	277.140	270.800	21.600

Table S4: adsorption isotherm experimental data for Compound **3**

C0	Ce (mg/L)			qe (mg/g)			Mean qe	SD
(mg/L)	rep 1	rep 2	rep 3	rep 1	rep 2	rep 3	(mg/g)	(mg/g)
25.000	15.169	15.291	16.055	98.310	97.090	89.452	94.951	4.801
50.000	29.428	30.001	29.584	205.720	199.991	204.160	203.290	2.962
75.000	26.545	25.963	26.005	484.550	490.370	489.950	488.290	3.246
100.000	34.287	35.185	34.844	657.130	648.150	651.564	652.281	4.533
150.000	78.795	78.903	79.003	712.050	710.970	709.967	710.996	1.042
200.000	130.008	129.727	129.480	699.920	702.735	705.200	702.618	2.642
250.000	180.785	180.924	179.941	692.150	690.765	700.590	694.502	5.318